This is to certify that the

thesis entitled

STRESS ANALYSIS OF GROOVED
AND THREADED DIE CASTING MACHINE TIE BARS

presented by

Frank De Roos Baron

has been accepted towards fulfillment
of the requirements for

MS degree in Mech. Engr.

Clark Radcliffe
Major professor

Date Feb. 21, 1983

STRESS ANALYSIS OF GROOVED

AND THREADED DIE CASTING MACHINE TIE BARS

By

Frank De Roos Baron

A THESIS

Submitted to
Michigan State University
in partial fulfillment of the requirements
for the degree of

MASTER OF SCIENCE

Department of Mechanical Engineering

1983

ABSTRACT

STRESS ANALYSIS OF GROOVED
AND THREADED DIE CASTING MACHINE TIE BARS

By

Frank De Roos Baron

The analysis of stresses in die casting machine tie bars is a specific example of the general case of the stress analysis of projection loaded members. Other examples would be gears and shafts with keyways. The two types of bars analyzed are a threaded bar with a nut and a grooved bar with a split collar. The stresses were analyzed to increase fatigue life.

Two finite element programs were used to analyze the stresses. One used linear elements, the other quadratic elements. Previously published empirical and analytical methods were also used. The maximum stresses obtained were used to calculate factors of safety.

The finite element analyses indicate that a radius fillet is the best design for the grooved bar. The threaded bar analyses indicate that the stress concentration factors for nut and bolt combinations may be higher than generally believed.

ACKNOWLEDGMENTS

I would like to thank my advisor Dr. Clark Radcliffe for his encouragement and help in organizing this material.

I would also like to thank Mr. David Kanistanaux for his help in the tensile testing area.

Finally, thanks go to Dr. Larry Segerlind for his guidance on the finite element program.

TABLE OF CONTENTS

LIST OF TABLES

LIST OF FIGURES

LIST OF SYMBOLS

a	See Figure 2.2
b	See Figure 2.2
c	Reducing Factor for Combined Stress
d	Neck Diameter of Grooved Bar
d_m	Minor Diameter of Threaded Bar
D	Outside Diameter
D_m	Mean Diameter of Thread
D_3	Equivalent Diameter of Nut
e	See Figure 2.2
F.S.	Factor of Sagety
h	Depth of Thread
h_e	Effective Depth of Thread
H	Load Concentration Factor
k	Correction for Grooved Bar
K_c	Corrected Stress Concentration Factor
K_o	Projection Loaded Stress Concentration Factor
K_t	Axial Loaded Stress Concentration Factor
L	Length of Nut
m	See Figure 2.4
p	Pitch of Thread

P	Axial Load
r	Radius of Fillet
R	Resultant Load
t	Thickness of Projection
w	$1/p$
x	Height of Fundamental Triangle
β	See Figure 2.2
δ	Depth Correction Factor
γ	Friction Angle
μ	Coefficient of Friction
σ	Poisson's Ratio
σ_{avg}	Average Nominal Stress
σ_b	Bending Stress
σ_c	Combined Stress
σ_e	Endurance Limit
σ_r	Range of Nominal Stress From Average
σ_t	Tensile Stress
σ_{yp}	Yield Strength

CHAPTER ONE

INTRODUCTION

This paper examines the stress concentration factors and fatigue resistance of various tie bar designs. The tie bar is a typical example of a machine member in tension. The methods presented are also used to analyze stresses in conventional nut and bolt combinations.

A die casting machine is a press which holds two die halves together. Molten metal is injected under high pressure into the cavities of the die halves to form the desired part. These high injection pressures dictate the need for large forces to hold the die halves together. Die casting machines are rated by the force that can be applied to the die halves. Ratings range from 90 to 3000 tons.

The basic parts of a die casting machine are the three plates, the toggles, the four tie bars, and the tie bar fasteners. The plates are all approximately square and have a hole bored in each corner. The tie bars slip through these holes and are fastened on the ends.

Figure 1.1 shows how the toggles slide the movable plate along the tie bars to squeeze the die halves together. The spacing on the machine is such that the die halves touch just before the toggles are fully extended. After the die halves touch, the toggles continue to extend, pushing the plates up against the fasteners and putting the tie bars

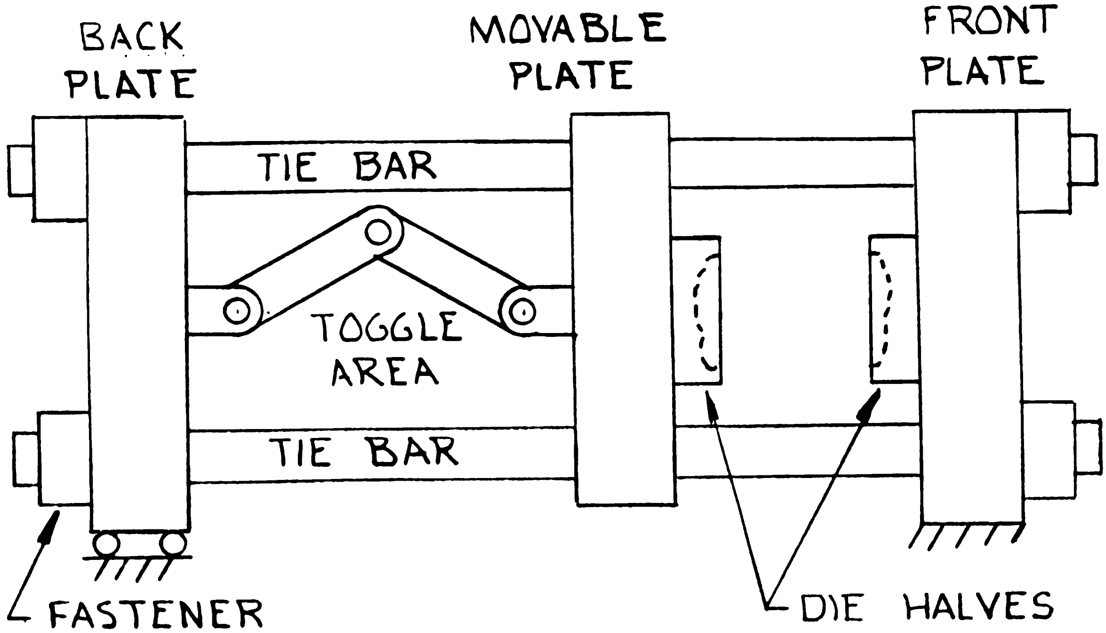

Figure 1.1 Simplified Die Casting Machine

in tension. The tie bars have to stretch to let the toggles reach their full extension. This tensile load in the tie bars is what provides the force that holds the die halves together. Since there are four tie bars, the load per bar is the rated tonnage divided by four. Once the toggles are fully extended and the tie bars stretched, the molten metal is injected to make a part. The toggles then retract so the part can be removed, and the cycle begins again. Because of the cyclic load the tie bars are subject to fatigue failure in the fastener area.

The first die casting machine was introduced in 1908. Early machines had Whitworth or American National threads machined on the ends of the tie bars. A solid nut was used as a fastener. Acme threads were used later to ease nut removal (Figure 1.2). The fasteners must be removable to allow for adjustment in machine spacing. This adjustment is necessary if dies are changed or if there is thermal growth of the die. A later development in threaded bars with Acme threads was the use of a tapered nut to improve load distribution among the threads. The last bar fastening method developed was to machine a groove in the tie bar and bolt a split collar around the groove.

The tie bar is a specific example of a member being put in tension by projection loading (Figure 1.3). The projection loading of threads was of particular interest in the mid 1940's when the unification of threads was being studied. Thread analysis took two forms at this time (1) testing and analysis of a specific thread form, (2) use of mathematical and empirical formulas to analyze thread forms in general. M. Hetenyi used testing and analysis in 1943 when he performed three dimensional photoelastic testing on a 1 inch diameter Whitworth nut and bolt combination. Hetenyi's testing showed that with a cylindrical

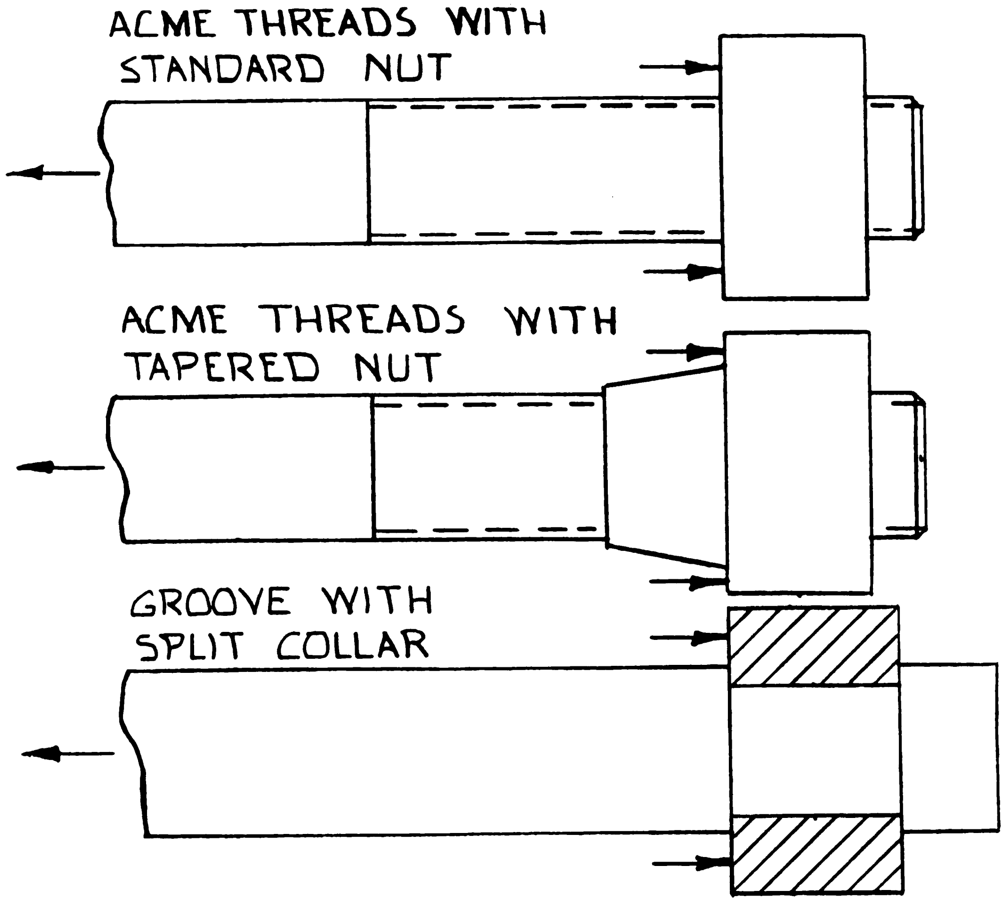

Figure 1.2 Types of Tie Bars

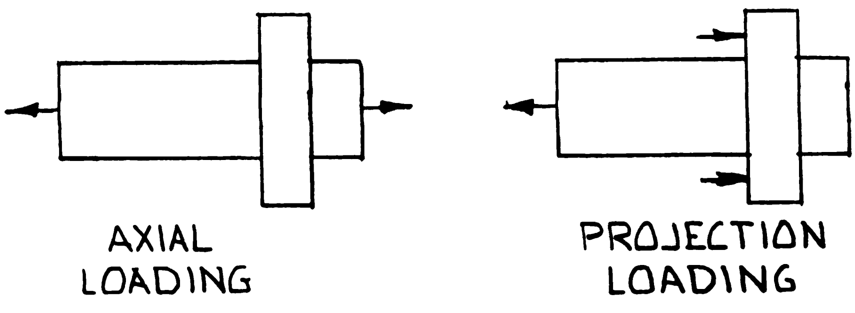

Figure 1.3 Types of Loading

nut the Whitworth threads had a stress concentration factor of 3.85 based on outside diameter. Use of a tension nut reduced this value to 3.00[2]. If the stress concentration factor is based on minor diameter, the values are 2.70 and 2.10 respectively[2]. The stress concentration factors derived by Hetenyi are the values generally used today for Whitworth or Unified National threads.

D.G. Sopwith used a more general approach in 1948 when he used a mathematical analysis to calculate the distribution of load in a nut and bolt of arbitrary thread form. There is not a uniform distribution due to the differences in strain between the nut and bolt. When the nut and bolt are loaded, the bolt is in tension while the nut is in compression. This causes changes in the pitch of the nut and bolt relative to each other and consequently a large percentage of the load is carried by the first thread. Sopwith's mathematical results showed good agreement with the experiments performed by J.N. Goodier in 1940[2]. Goodier loaded a 1-1/4 inch American National nut and bolt, measured the axial and radial displacements, and from these calculated the load distribution[2].

In 1948, R.B. Heywood derived empirical results to calculate the stress in the fillet of a loaded projection. Heywood's results were based on his photoelastic experiments which included work on various thread forms. He used the mathematical results of Sopwith to determine the load distribution in a Whitworth nut and bolt combination, and the mathematically derived charts of Neuber to determine the stress concentration factor of a multiply grooved shaft in tension (no projection load). The preceeding mathematical results were used with his empirical results to determine the maximum tensile stress in the thread fillet. From this he calculated the stress concentration factor for Whitworth threads to be 5.2 based on minor diameter[1]. This is substantially higher than Hetenyi's results. In 1952, Brown and Hickson obtained a stress concentration factor of 4.8 based on minor diameter from their three dimensional photoelastic testing of a 2 inch Unified National nut and bolt combination[2]. These mixed results show that exact stress concentration factors for nut and bolt combinations are not well determined.

The work presented here calculates the stress concentration factors for the eight bars listed below.

Bar #1 .500 min. dia., .688 maj. dia.

Bar #2 .750 min. dia., 1.00 maj. dia.

Bar #3 1.00 min. dia., 1.38 maj. dia.

Bar #4 5.20 min. dia., 6.75 maj. dia. (600 ton machine)

Bar #5 1/2-13 UNC thread

Bar #6 3/4-10 UNC thread

Bar #7 1-8 UNC thread

Bar #8 6.50 dia 4 thds/in Acme thread (650 ton machine)

All dimensions in inches

Bars one through four are the grooved type, while bars five through eight are the threaded type. Bars four and eight have dimensions of tie bars in use today.

The work discussed here includes two approaches, empirical methods and finite element methods. Chapter Two of this paper follows Heywood's procedure quite closely. Sopwith's results are used to determine the distribution of loading in the threaded bars and Neuber's charts are used to determine the stress concentration factors of multiply grooved bars in tension. This information is used in Heywood's results to determine the maximum tensile stress. Heywood also did photoelastic testing of members similar to the grooved tie bars, so his results could be applied directly to determine the maximum tensile stress in the grooved tie bars. These maximum stresses are used to calculate stress concentration factors for the two types of bars. Chapter Three determines the maximum tensile stress in the bars by using finite element analysis. The maximum stresses are used to calculate stress concentration factors. Chapter Four uses the stress concentration factors in the Soderberg equation[5] to determine factors of safety based on fatigue strength for bars four and eight. Chapter Four includes results derived from testing model tie bars on a tensile testing machine.

CHAPTER TWO

ANALYTICAL AND EMPIRICAL FORMULATIONS

2.1 INTRODUCTION

The calculation of the maximum tensile stress in the various tie bar designs using the empirical results of R.B. Heywood[1], the mathematical results of D.G. Sopwith[4], and the mathematical charts of H. Neuber[2] is discussed in this chapter.

2.2 THE GROOVED BAR

Projection loaded members are frequently encountered in machine design. The grooved tie bar (Figure 1.2) is a specific example. The projection is the shoulder created by machining a groove in the end of the tie bar. Other types of projection loaded members include gears, threaded bars, and shafts with keyways.

R.B. Heywood did photoelastic testing of projection loaded members in the mid 1940's in order to derive empirical results that can be used to calculate the tensile stress in the fillet of a loaded projection. Heywood used his results to analyze the stresses in bolt heads which are similar to the geometry of the grooved tie bar. His results are used here to calculate the maximum tensile stress in the fillet of the grooved tie bar.

Heywood observed from his photoelastic testing that when a shaft is in tension due to a projection load, there are two factors that produce stress in the fillet region of the projection. There will be a stress component due to the axial load, and a stress component due to projection load as shown in Figure 2.1[1]. The stress due to projection load will be examined first.

Heywood observed that there are three factors to be considered when calculating the stress due to projection load. These factors are: Bending stress, proximity of the load to the fillet, and the fillet geometry. With the dimensions shown in Figure 2.2, Heywood developed Equation 2-1 to fit his photoelastic data[1].

$$\sigma_b = \underbrace{\left[1 + 0.26\left(\frac{e}{r}\right)^{0.7}\right]}_{\text{fillet geometry effect}}\left[\underbrace{\frac{1.5a}{e^2}}_{\text{bending stress}} + \underbrace{\sqrt{\frac{0.36}{be}}\left(1 + 1/4\sin\gamma\right)}_{\text{proximity stress}}\right]\left(\frac{P}{t}\right) \qquad (2\text{-}1)$$

The bending stress term in Equation 2-1 is similar to the Lewis formula for gear teeth. It represents the stresses in the fillet due to the moment created by P (Appendix A). The proximity stress term is the stress due to the proximity of the load to the fillet and is attributed to the transitional strains between loaded and unloaded areas. When one section is under load, the unloaded section adjacent to it will have strains induced in it as shown in Figure 2.3. The fillet geometry effect term represents the effect of the radius of the fillet.

Heywood's results can be used for a wide range of geometries[1]. In the case of a long projection, b, gets large, and the proximity term diminishes (Figure 2.2). In the case of a short projection, a, gets small and the moment term diminishes (Figure 2.2). If a large radius

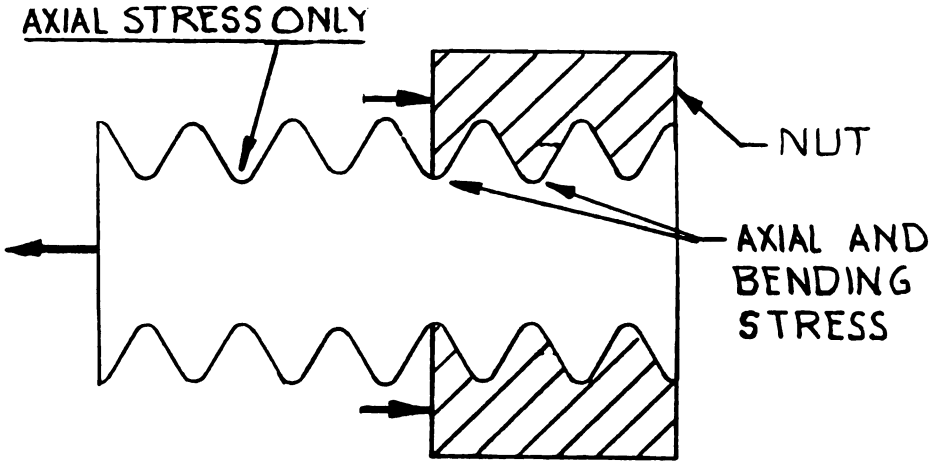

Figure 2.1 Stresses in Projection Loaded Shafts

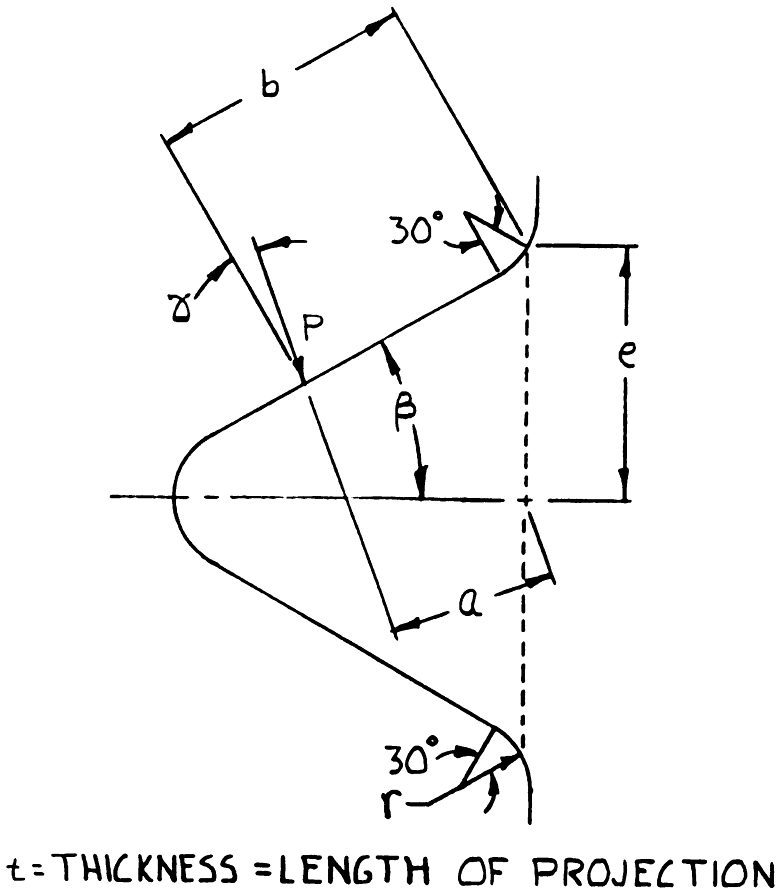

Figure 2.2 Dimensions for Using Heywood's Results

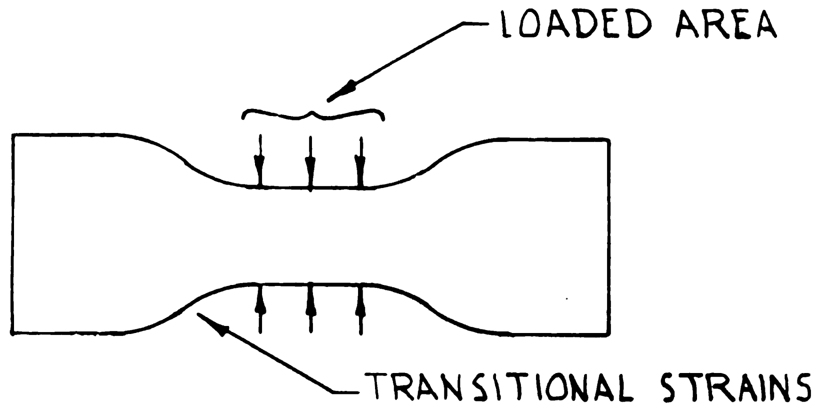

Figure 2.3 Exaggerated Strains

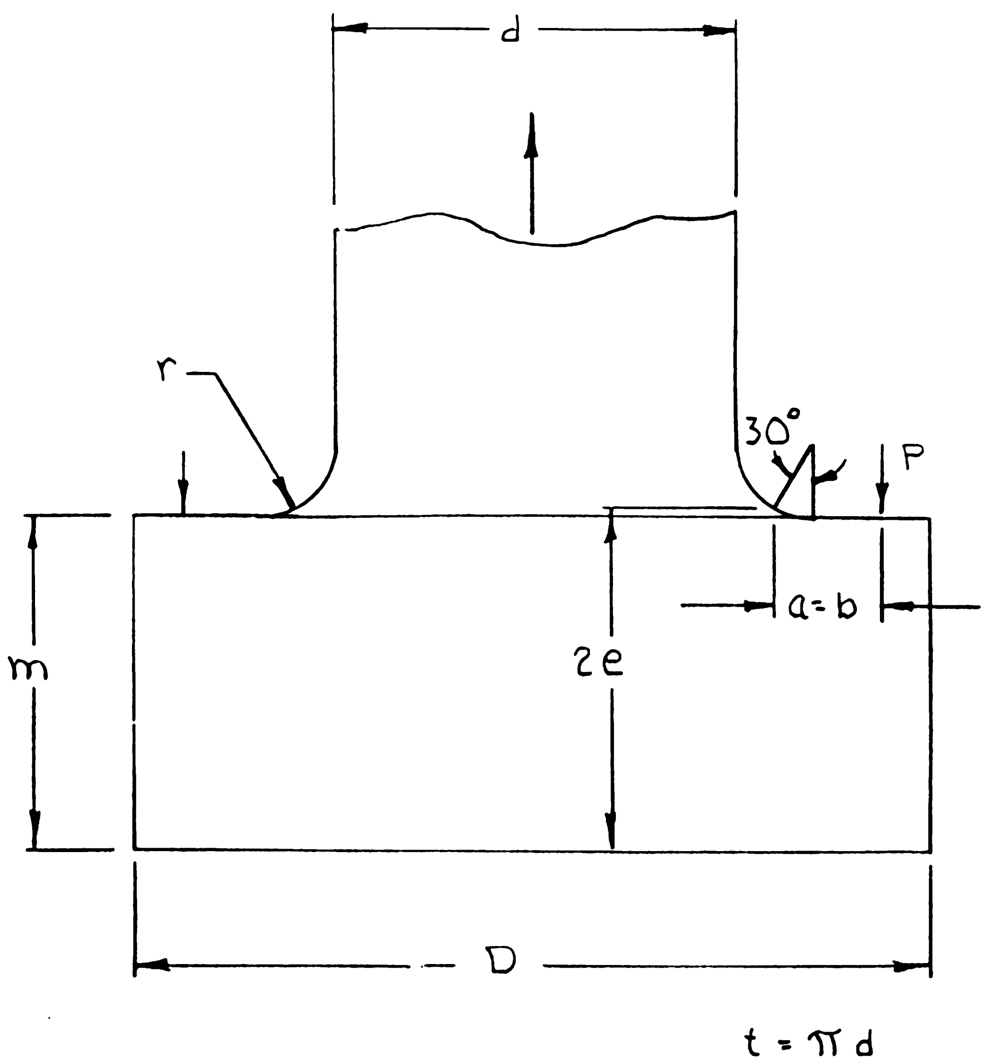

Figure 2.4 Grooved Bar Dimensions

fillet is used, the geometry effect term is reduced, while smaller radii tend to increase stress.

The dimensions required to apply Heywood's general projection formula results specifically to the grooved bar are shown in Figure 2.4. The thickness, t, equals, πd, the circumference of the smallest diameter[1].

Comparisons of Heywood's formulations with photoelastic testing done by Hetenyi on similar members, showed Heywood's results for stresses to be consistently lower. This was attributed to the significant differences in geometry between the conventional projection and the grooved tie bar geometry. Heywood modified the fillet geometry effect term as shown in Equation 2-2 to correct this[1].

$$\text{geometry effect} = [1 + 0.26(\tfrac{e}{r})^{0.7}k] \qquad (2\text{-}2)$$

$$\text{where } k = \frac{5.6m/d + 1}{2.0m/d + 1} \qquad (2\text{-}3)$$

see Figure 2.4 for dimensions

Heywood derived Equation 2-4 by use of the dimensions in Figure 2.4 and the correction shown in Equation 2-2. Equation 2-4 is used to calculate the stress due to projection load in the grooved bar.

$$\sigma_b = [1 + 0.26(\tfrac{e}{r})^{0.7}(\frac{5.6m/d + 1}{2.0m/d + 1})][\frac{1.5a}{e^2} + \sqrt{\frac{0.36}{ae}}]\frac{P}{\pi d} \qquad (2\text{-}4)$$

since $a = b$ and $\gamma = 0$

The second source of stress in the fillet is the stress component due to axial load. Equation 2-5 gives the maximum stress in an axially loaded shouldered shaft. It is obtained by multiplying the nominal stress by the stress concentration factor, K_t, obtained from Figure 2.5[2].

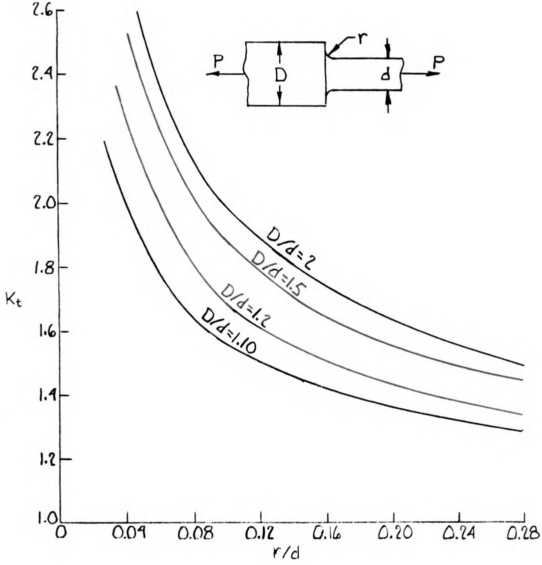

Figure 2.5 Stress Concentration Factors, K_t for Shouldered Shafts in Tension [2]

$$\sigma_t = \frac{K_t P}{\pi(d/2)^2} \tag{2-5}$$

The stress in the fillet is a combination of stress due to projection load (Equation 2-4) and axial stress (Equation 2-5). Addition of the two stress components will give a value of stress that is too high because the points of maximum stress due to the two types of loading occur at different locations on the fillet. Photoelastic experiments by Heywood showed that the point of maximum stress due to bending occurs 30 degrees from the tangent point of the radius[1]. The point of maximum stress due to axial load occurs at the bottom of the fillet[1] (Figure 2.6). The relationship that Heywood developed to calculate the combined stress is given in Equation 2-6[1].

$$\sigma_c = \sigma_t + \frac{\sigma_b}{1 + c\ \sigma_t/\sigma_b} \tag{2-6}$$

The coefficient, c, is reducing factor based on the distance between the two points of maximum stresses[1]. Heywood expressed it as a function of the angle between these points as given in Equation 2-7.

$$c = \left(\frac{60 - \beta}{44}\right)^2 \tag{2-7}$$

β in degrees

Heywood's analysis is intended for a grooved tie bar with a circular fillet. His photoelastic testing indicated that a streamline fillet (Figure 2.7), will reduce the maximum tensile stress in the fillet by 25 percent. The results of the above analysis (Appendix B) for the various sizes of grooved bars are shown in Table 4.1.

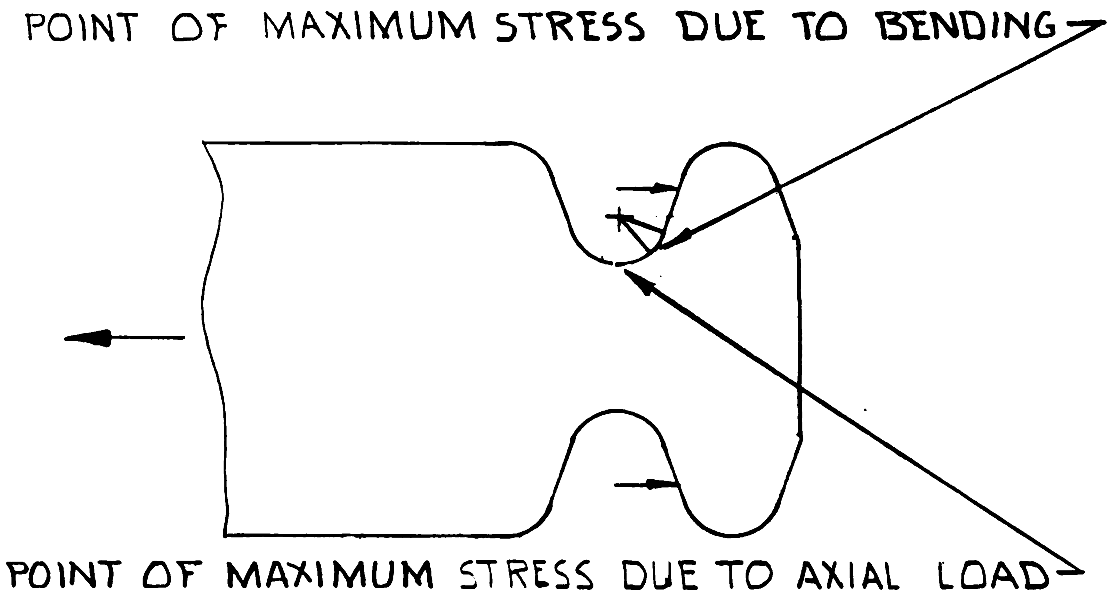

Figure 2.6 Location of Maximum Stresses

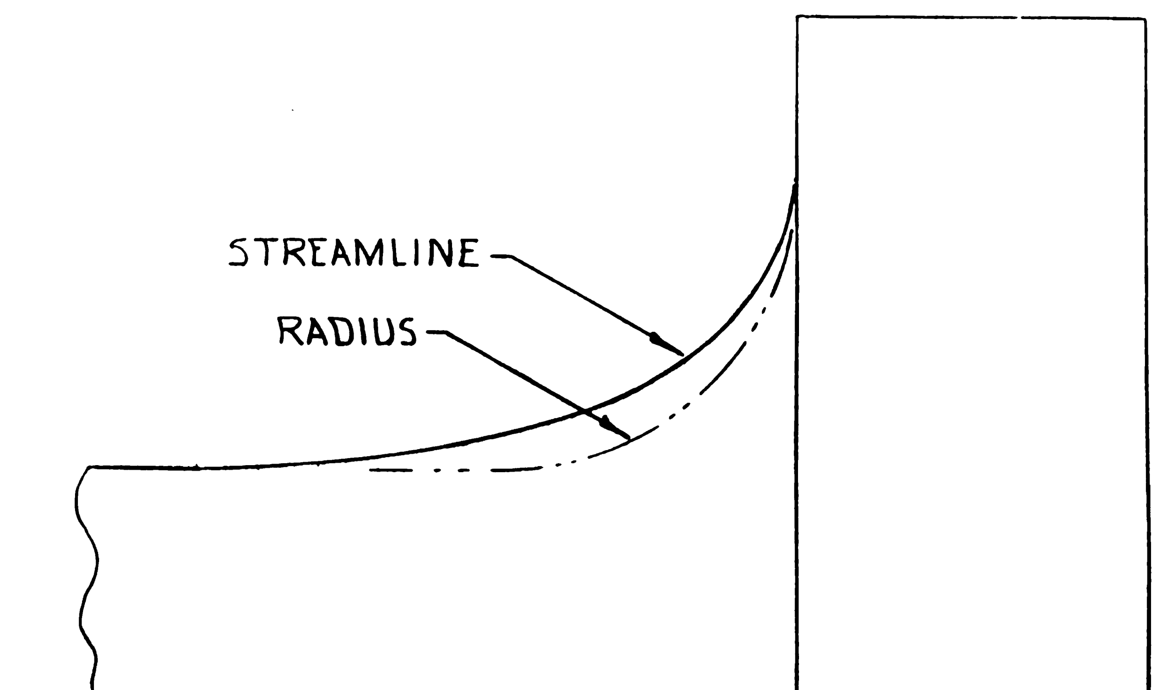

Figure 2.7 Streamline Fillet

2.3 THE THREADED BAR

Because of the difficulties involved in determining the distribution of load between the threaded bar and nut, analyzing the threaded bar is a more complex problem than analyzing the grooved bar. When the bar and nut are loaded, the nut is compressed, shortening its pitch. The bar, however, is stretched, lengthening its pitch. This creates disparities in strain, which concentrate a large percentage of the load at the first thread. The load carried by the first thread is determined by Sopwith's analysis. This information is then used in Heywood's projection formula to calculate the stress due to thread load (bending). Stress due to axial load can be determined by using the charts of Neuber. The combined stress is then obtained by using Equation 2-6, which was also derived by Heywood.

Sopwith analyzed the strains produced in a loaded threaded bar and nut, and found that the load carried by the first thread is a function of length of nut, equivalent outside diameter of nut, pitch of thread, and the ratio of thread depth to height of fundamental triangle (Figure 2.8).

The assumptions made by Sopwith are listed here[4].

1. Manufacturing errors in pitch and flank angle can be neglected.
2. Stress concentrations at the root of the thread can be neglected since they are local in nature and will not affect overall strain.
3. The thread can be treated as a tapered cantilever built in at the root diameter.
4. The load is concentrated at mid-depth on this cantilever because of symmetry (Figure 2.9).
5. The radius of the root does not affect the stiffness of the threads.

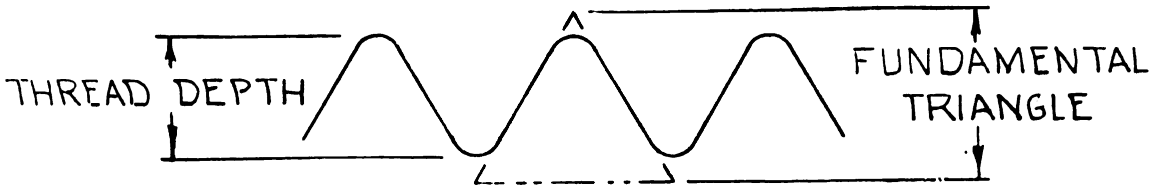

Figure 2.8 Fundamental Triangle

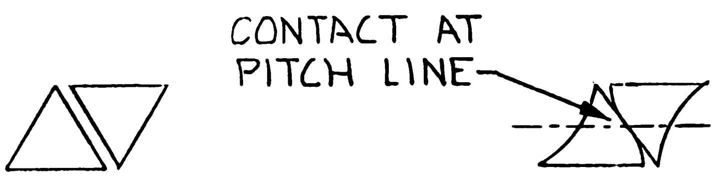

Figure 2.9 Deflection of Thread

The formulas resulting from Sopwith's studies are given in Appendix C. The dimensions required are shown in Figure 2.10[4].

The final result of Sopwith's analysis is the value H, which is by definition the maximum load per length of helix divided by the average load per length of helix. This ratio is used to calculate stress due to thread load.

The axial load plus frictional forces combine to form the resultant force, R, given in Equation 2-8 and shown in Figure 2.11[4].

$$R = P(\sec(\beta-\gamma)) \tag{2-8}$$

β = flank angle (Figure 2.2)
γ = friction angle

The average load per length of helix is given by Equation 2-9.

$$\left(\frac{R}{t}\right)_{avg} = \frac{R}{\pi(d_m)(L)(p)} \tag{2-9}$$

Here $\pi(d_m)$ is the circumference of the minor diameter[1], (L) is the length of nut and (p) is the pitch of the threads.

The maximum load per length of helix is given by Equation 2-10.

$$\left(\frac{R}{t}\right)_{max} = H\left(\frac{R}{t}\right)_{avg} \tag{2-10}$$

The stress due to thread load, σ_b, is obtained by substituting $H(R/t)_{avg}$ for P/t in Equation 2-1 and is given by Equation 2-11[1].

$$\sigma_b = [1 + 0.26(\tfrac{e}{r})^{0.7}][\frac{1.5a}{e^2} + \sqrt{\frac{0.36}{be}}(1 + 1/4\sin\gamma)]H(\tfrac{R}{t})_{avg} \tag{2-11}$$

The stress concentration factor of a multiply grooved shaft in tension must be found to determine the fillet stress component due to axial load. The stress concentration factor is higher in a shaft with

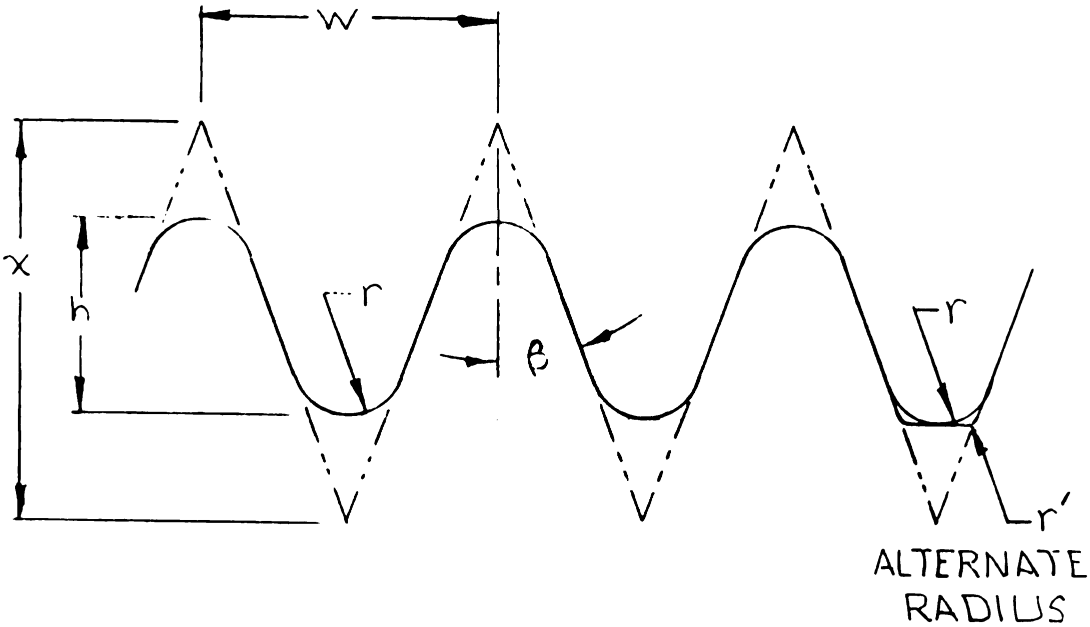

Figure 2.10 Sopwith's Analysis Dimensions

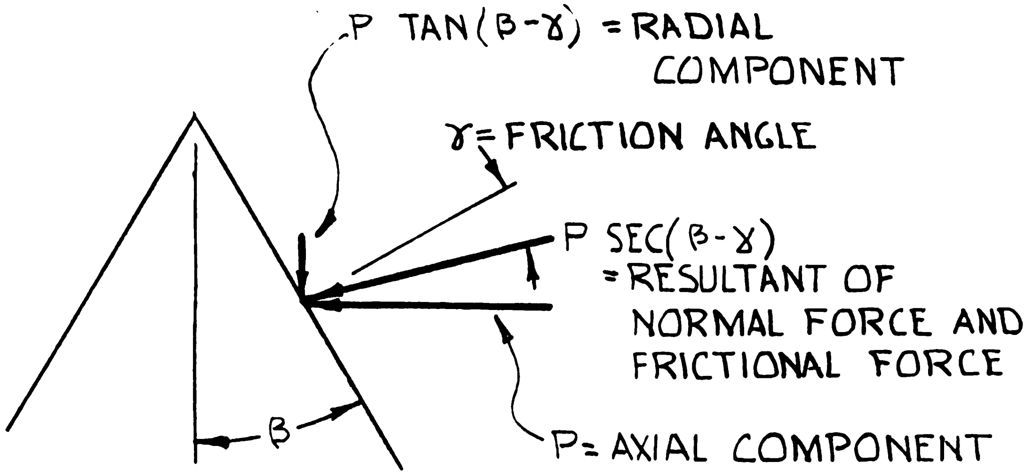

Figure 2.11 Load Components

a single groove than it is in a shaft with multiple grooves. Figure 2.12 is used to determine the correction factor δ, which is used to calculate h_e, the depth of a single groove that yields the same stress concentration factor as multiple grooves (Equation 2-12).

$$h_e = \delta h \tag{2-12}$$

where h = depth of multiple grooves
h_e = effective depth for single groove

The stress concentration factor for a grooved shaft in tension, K_t, is now determined from Figure 2.13. The parameters needed for Figure 2.13 are the minor diameter d, and the major diameter D, which is equal to $d+2(h_e)$.

Figure 2.13 is intended for straight-sided grooves. The angled flanks of the threads reduce the stress concentration factor. The value of K_t can be corrected by Equation 2-13[1].

$$K_c = 1 + (K_t-1)\left[1 - \left(\frac{2\beta}{180}\right)^{1 + 2.4\sqrt{r/h_e}}\right] \tag{2-13}$$

β in degrees

The tensile stress for the threaded rod is now given by Equation 2-14.

$$\sigma_t = \frac{K_c P}{\pi(d_m/2)^2} \tag{2-14}$$

The combined stress can now be calculated as it was in Equation 2-6, which is repeated here as Equation 2-15.

$$\sigma_c = \sigma_t + \frac{\sigma_b}{1 + c\ \sigma_t/\sigma_b} \tag{2-15}$$

$$\text{again } c = \left(\frac{60 - \beta}{44}\right)^2 \tag{2-16}$$

β in degrees

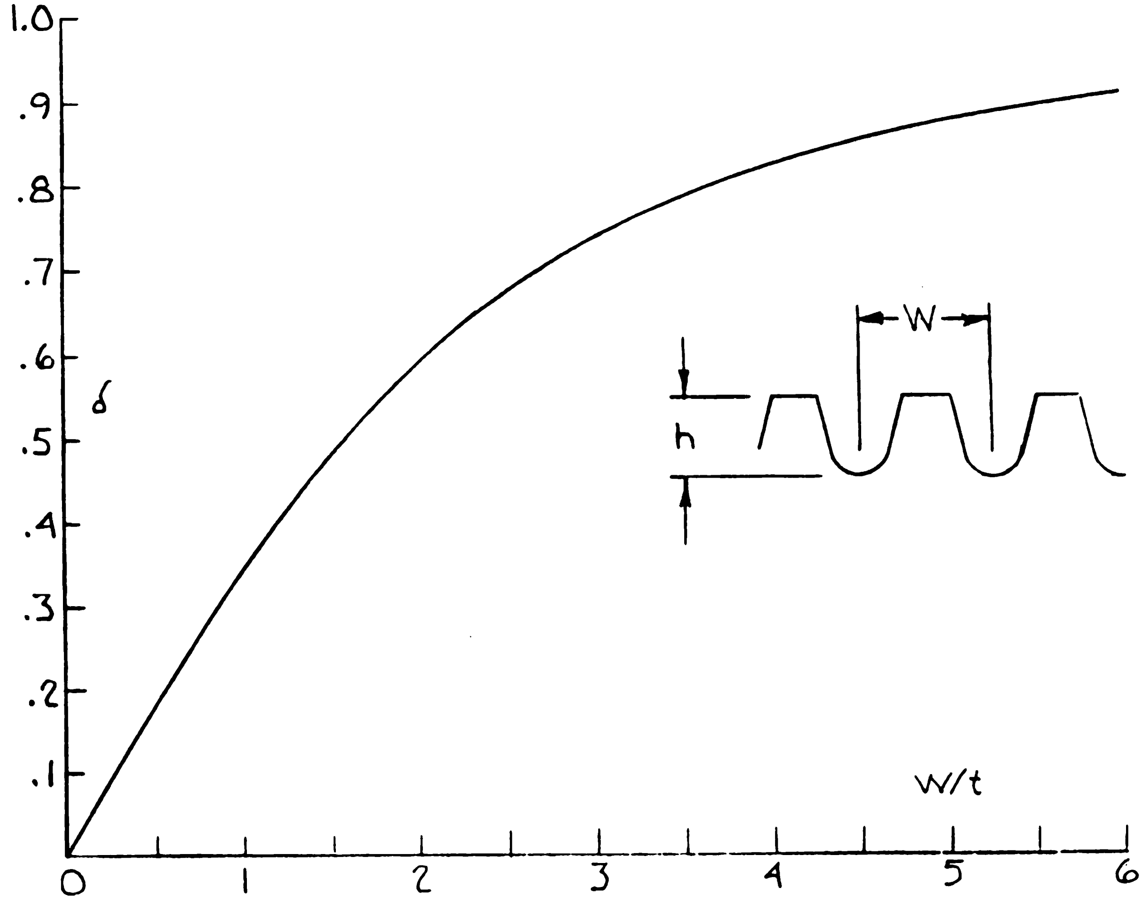

Figure 2.12 Depth Correction Factor, δ[2]

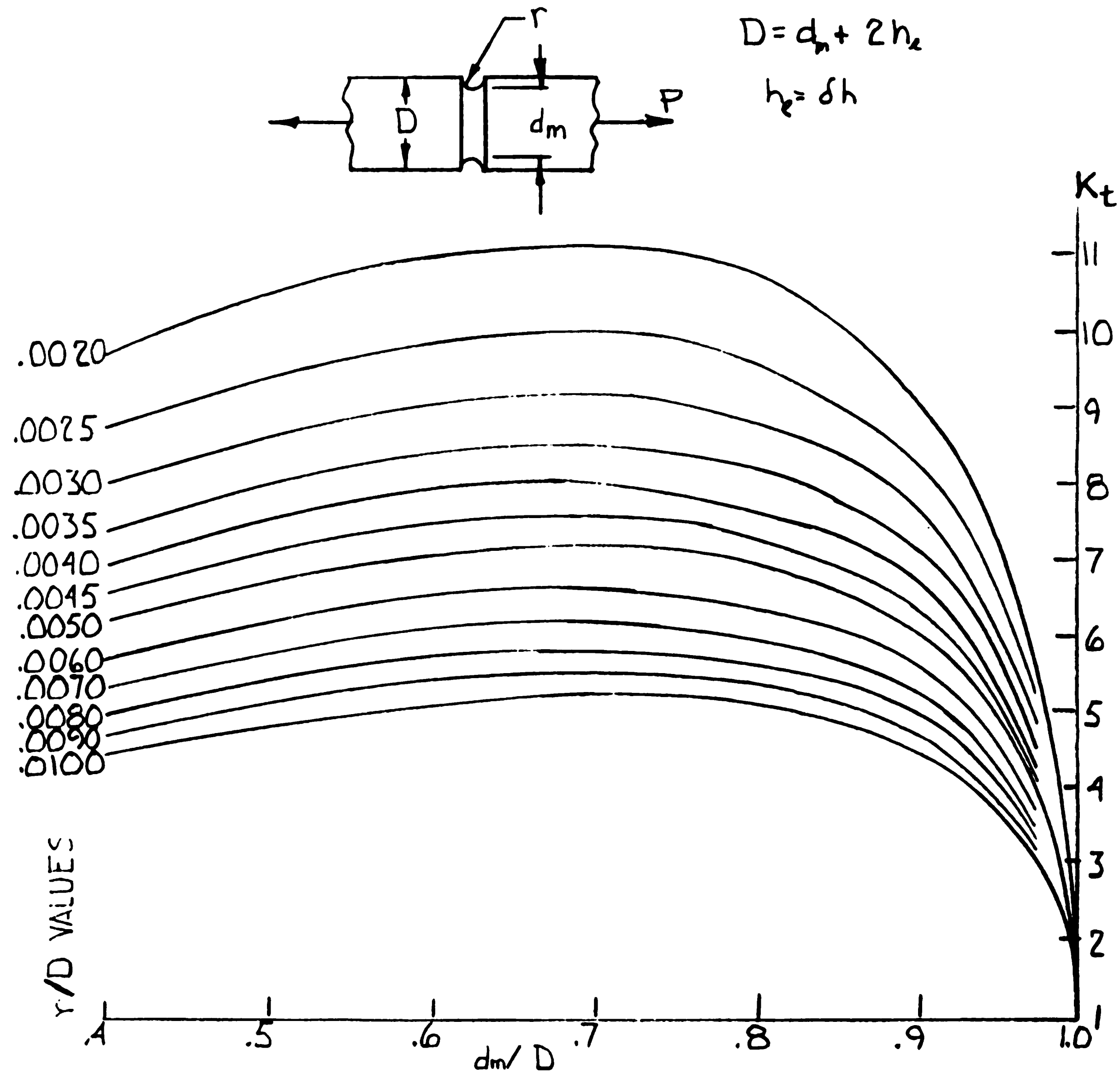

Figure 2.13 Stress Concentration Factors, K_t, for Grooved Shafts in Tension [2]

The analysis above is intended for a standard nut. One way of improving the distribution of loading is to use a tapered nut of the design shown in Figure 1.2. The taper improves load distribution by making the nut more flexible near the first threads which allows more load to be carried by the last threads. Tests by Hetenyi show that a 30 percent improvement in load distribution can be achieved by this design[2]. The combined stress can be divided by the nominal stress to obtain the projection loaded stress concentration factor.

The results of the analysis on the eight bars listed in Chapter One are tabulated in Table 4.2. Calculations pertaining to these analyses are shown in Appendix C. This chapter has outlined anayltical and empirical methods for stress analysis. Chapter Three will outline the finite element method.

CHAPTER THREE

FINITE ELEMENT ANALYSIS

3.1 INTRODUCTION

The grooved tie bar is an example of an axisymmetric body. The loading and geometry are functions of the radial and axial coordinates only. It is also assumed that the threaded bar can be approximated as an axisymmetric body by using axisymmetric grooves instead of helical threads. The torsional effects due to the loading of the helical threads are assumed to be small compared to the stresses produced by the projection loading of the threads. Because of the axisymmetric nature of the body, it can be analyzed using two dimensional finite element methods. The results of this analysis are the three dimensional stress components from which the principal stresses and maximum shear stress can be determined.

3.2 PROGRAM OVERVIEW

The first step in the finite element method is to discretize the region being examined into finite areas called elements. The points that are specified around the boundaries of each element are called nodes. The displacement at equilibrium is calculated for each node.

Polynomials called shape functions are used to interpolate displacements within the elements. Two programs are used to analyze the stresses in the bars. The first uses first order shape functions, the second uses second order shape functions. The finite element analysis is based on the principle of minimum potential energy which states that when a loaded member is in its equilibrium position, its potential energy at a minimum. The potential energy is expressed as a function of the nodal displacements. The position of minimum potential energy is found by taking the derivative of the potential energy function with respect to the nodal displacements and setting it equal to zero. Setting the derivative equal to zero yields a set of simulataneous equations that can be solved to find the nodal displacements associated with the point of minimum potential energy. The element stresses are obtained from the nodal displacements. Equations 3-1 and 3-2 show these steps in matrix form.

$$\frac{\partial \pi}{\partial \{U\}} = [K]\{U\} - \{F\} = 0 \tag{3-1}$$

here π = potential energy
$\{U\}$ = nodal displacement vector
$[K]$ = stiffness matrix
$\{F\}$ = force vector

$$\{\sigma\} = [D][B]\{U\} - [D]\{\varepsilon_o\} \tag{3-2}$$

here $\{\sigma\}$ = stress vector
$[D]$ = material property matrix
$[B]$ = strain interpolation matrix
$\{\varepsilon_o\}$ = initial thermal strain vector

The linear shape functions and the matrices in Equation 3-2 are shown in Appendix E.

The first finite element analysis uses a modified version of a two dimensional linear elasticity program written by Dr. L. Segerlind of Michigan State University. Modifications to change the two dimensional program into an axisymmetric program include using linear triangular torus elements that are obtained by rotating the linear two dimensional triangular element 360 degrees around the axis of symmetry. The elements are termed linear because they use first order shape functions. One disadvantage of using linear elements is that the displacement gradients are constant across the entire element. Since σ_{rr}, σ_{zz}, and τ_{rz} are dependent on these gradients, they will also be constant across the entire element. This disadvantage can be overcome by using small elements in the areas where the stress is changing rapidly[3]. Other modifications to the two dimensional program include a new material property matrix, [D], a new initial thermal strain vector, $\{\varepsilon_o\}$, a new strain interpolation matrix, [B], and rewriting the shape functions in terms of r(radial coordinate), and z(axial coordinate)[3].

In order to determine the element stiffness matrix, $[k^{(e)}]$ integral (3-3) has to be evaluated[3].

$$[k^{(e)}] = \int_{vol} [B]^T[D][B]dV \qquad (3\text{-}3)$$

The matrix, [B], cannot be pulled out of the integral since it contains terms that are a function of the coordinates. This problem is resolved by evaluating [B] by using the r and z coordinates of the centroid of the element. This leads to an approximate solution, but one that is acceptable if small elements are used in areas where the stress is changing rapidly[3].

The second analysis used the ANSYS finite element software which is a product of Swanson Analysis Systems, Inc. The overall strategy of ANSYS is similar to the previous program, but quadratic triangular torus elements are used. The quadratic elements use second degree shape functions, so the constant displacement gradients are eliminated. Because of this, the higher order elements will yield more accurate results when using the same grid. In order to be able to see the trend of the results as the more accurate elements were used, the same grids are used in both analyses.

3.3 BOUNDARY CONDITIONS

In both the threaded and grooved tie bar, it is necessary to represent a surface pressure as concentrated loads applied at specific nodes. The following distribution is used in the linear program for the loading shown in Figure 3.1[3].

$$\{f_p\} = \frac{2\pi L_{12}}{6} \begin{bmatrix} (2R_1 + R_2)P_r \\ (2R_1 + R_2)P_z \\ (R_1 + 2R_2)P_r \\ (R_1 + 2R_2)P_z \end{bmatrix} \begin{matrix} \left.\vphantom{\begin{matrix} a \\ a \end{matrix}}\right\} \text{node 1} \\ \left.\vphantom{\begin{matrix} a \\ a \end{matrix}}\right\} \text{node 2} \end{matrix} \qquad (3\text{-}4)$$

The constants P_r and P_z are surface pressures, R_1 and R_2 are the radial coordinates of the nodes, and L_{12} is the distance between the nodes. One should note that a greater percentage of the load is applied to the node that has the largest radial coordinate. Figure 3.2 shows the reason for this load distribution. The two shaded rings are of the same thickness, but the outer ring has more area, so it would carry more load if a surface pressure were imposed on the circle.

The distribution of load on the threaded bars is accomplished by using information from Sopwith's thread analysis[4]. For each threaded bar the maximum load per length of helix is determined. This value is multiplied by the circumference of a typical thread. This product is

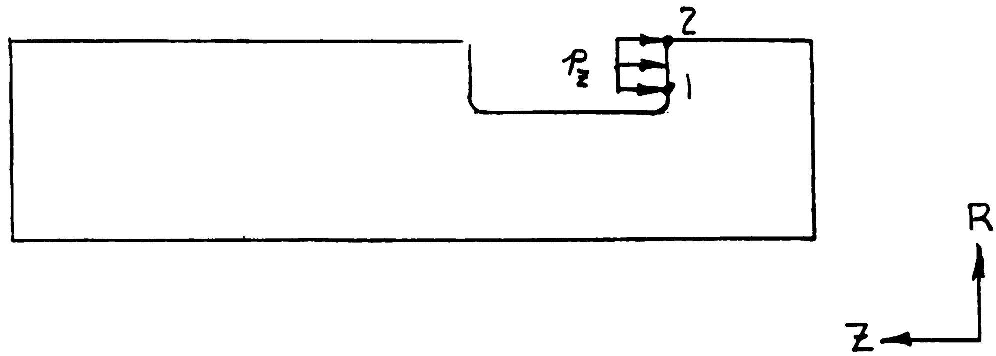

Figure 3.1 Surface Pressure

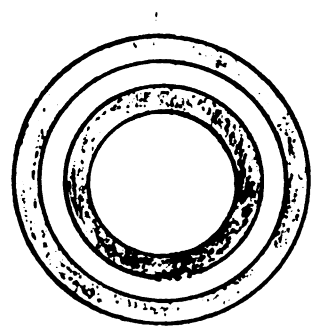

Figure 3.2 Surface Areas on an Axisymmetric Body

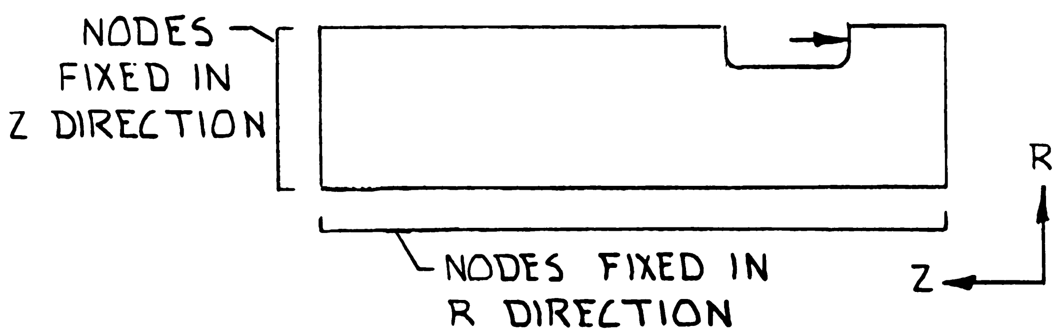

Figure 3.3 Boundary Conditions

assumed to be the load carried by the first thread. It is then determined what percentage of the total load this is. Each subsequent thread is then assigned this percentage of the remaining load. The remainder is divided equally among all threads. The load is discretized into R and Z components as shown in Figure 2.11[3].

Because of the symmetry in the bar geometry and loading, nodes along the axis are fixed in the R direction. Nodes along the unloaded end are fixed in the Z direction (Figure 3.3).

3.4 STRESS CONCENTRATION FACTORS

The finite element analysis can be used to determine stress concentration factors. The tie bar is analyzed subject to a constant load. Normally for a ductile material with constant load, the stress concentration factor is ignored because the material will yield locally and relieve itself[5]. In this finite element analysis, no provision has been made for yielding and the overstressed areas, which will be of interest if the member is to be subjected to a cycling load, are pointed out.

The results of the finite element analysis on the various geometries are in Tables 4.1 and 4.2. Grids for the different bars are shown in Figures 3.4 through 3.9.

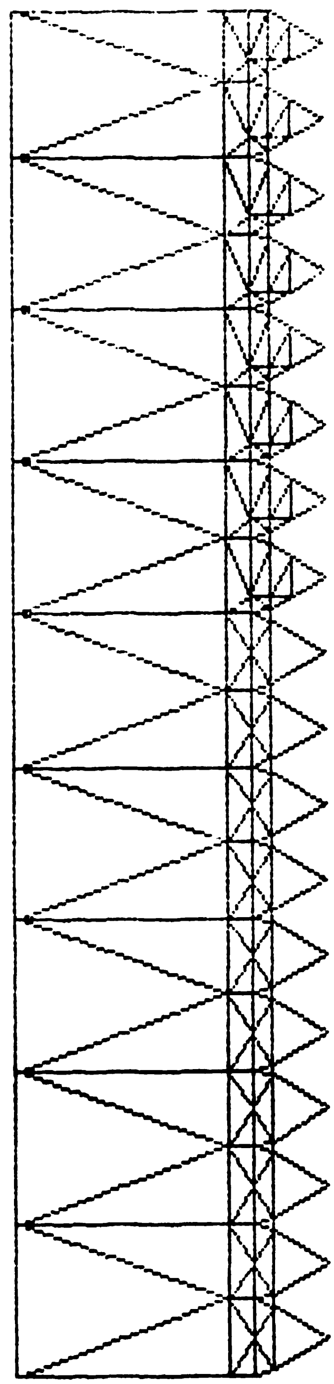

Figure 3.4 Typical Grid for UNC Threaded Bar

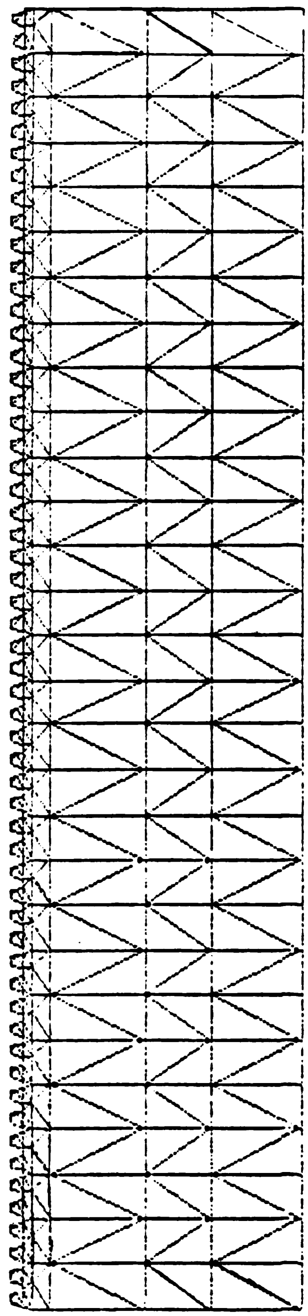

Figure 3.5 Grid for Acme Threaded Bar

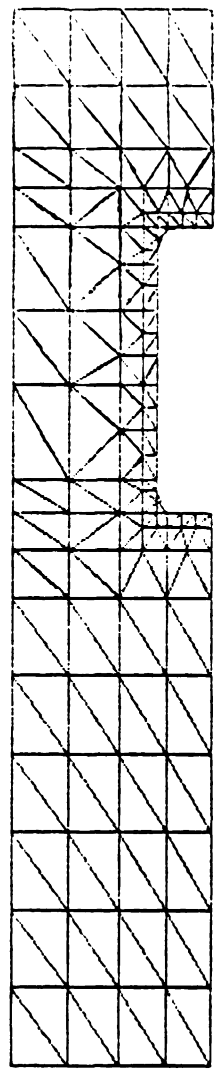

Figure 3.6 Typical Grid for Small Grooved Bar

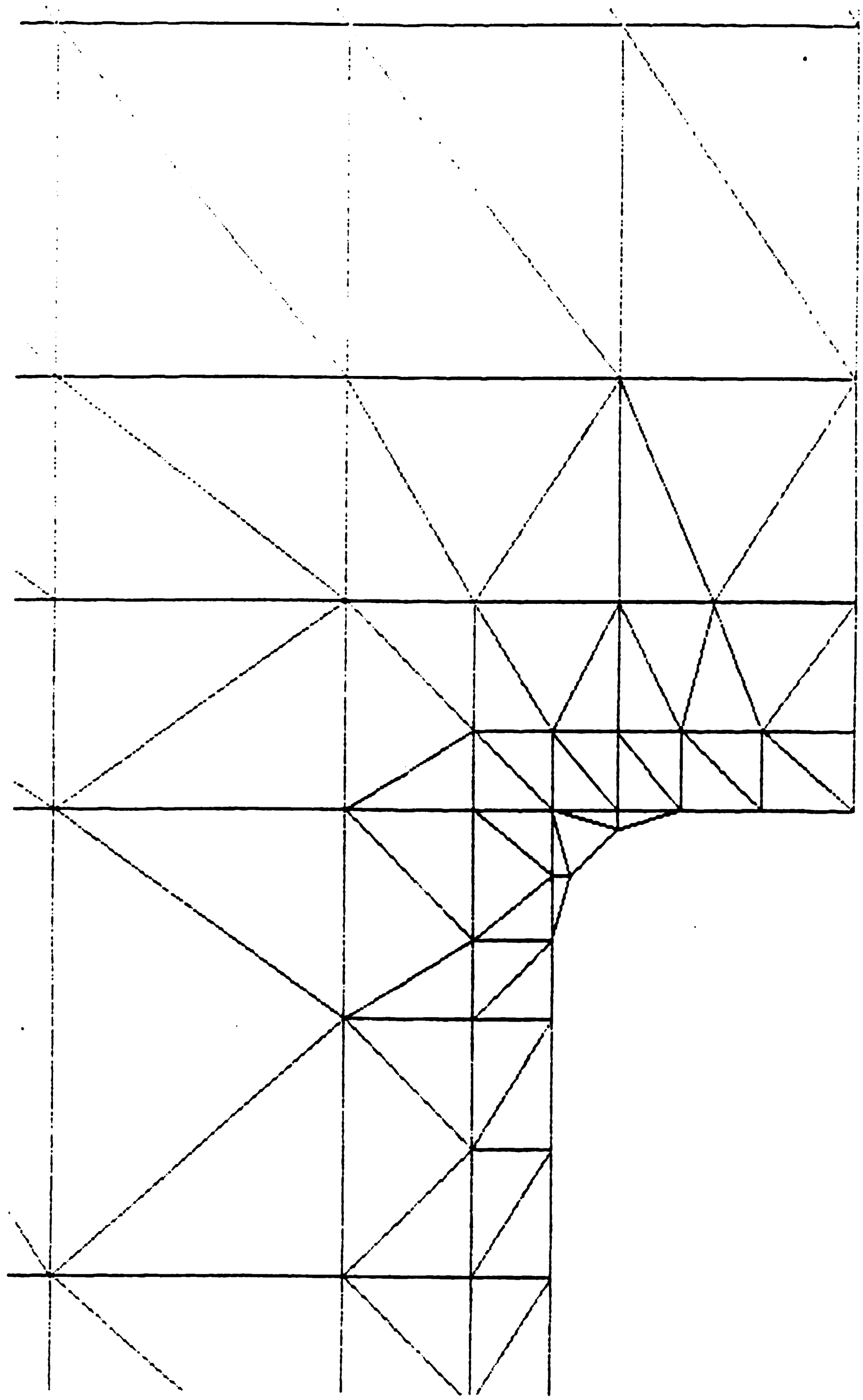

Figure 3.7 Detail of Radius for Small Grooved Bar

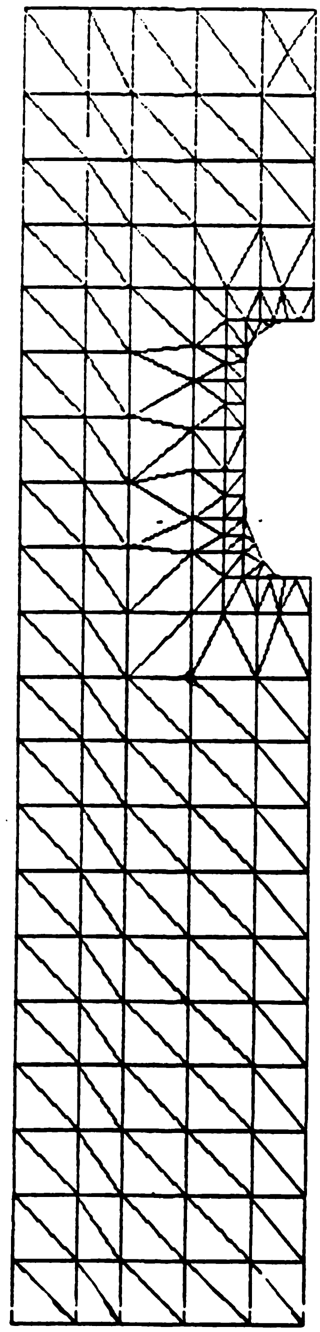

Figure 3.8 Grid for 6.75 O.D. Grooved Bar

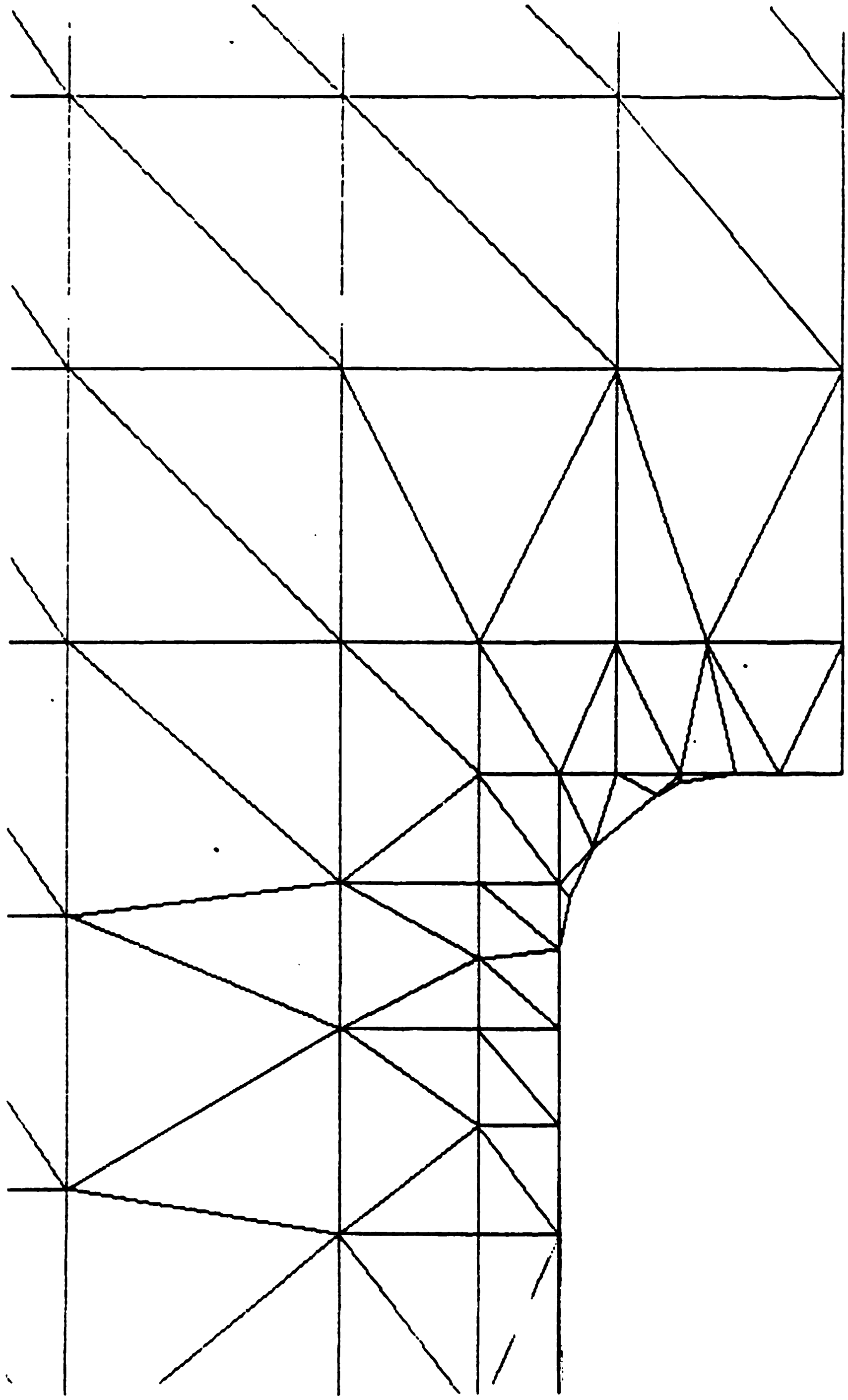

Figure 3.9 Detail of Radius Fillet, 6.75 O.D.

CHAPTER FOUR

RESULTS

4.1 GROOVED BAR

The projection loaded stress concentration factors for grooved bars, K_o show good correlation between the empirical results and the quadratic finite element results for the three smaller bars (Table 4.1). The difference between the two methods ranges from 2.6 to 6.5 percent. The 6.75 in. O.D. bar with a radius fillet has a difference of 14.1 percent between the two methods. The finite element results for the 6.75 in. O.D. bar appear to be more accurate because a finer grid was used in the fillet area. The stress concentration factors increase when the more accurate quadratic elements are used, which indicates that the stresses from Heywood's results are low, and that the correction factor employed for the grooved bar is incorrect. Because of the small variations between the linear and quadratic finite element values for the 6.75 in. O.D. bar, it is assumed that a finer grid or higher order elements would not significantly effect the accuracy of the results. To determine K_o, Equations 4-1 and 4-2 are used.

$$\sigma_{nom} = \frac{P}{\pi(d/2)^2} \qquad (4\text{-}1)$$

$$K_o = \frac{\sigma_{max}}{\sigma_{nom}} \tag{4-2}$$

Two other fillet designs were tried on the 6.75 in. O.D. bar to attempt to lower the maximum stress. The first is the streamline design (Figure 4.1a) that Heywood claimed could lower the maximum stress by 25 percent. The finite element results show that the maximum stress is not lowered significantly because of the small radius near the load. A reversed streamline (Figure 4.1b) was tried in order to place a large radius near the load. This resulted in raising the maximum stress by 46 percent because of the small radius at the bottom of the fillet. The large difference between the finite element values indicate that the stress concentration factor may be higher than the quadratic finite element value for the reversed streamline.

The axial loaded stress concentration factors for shouldered shafts, K_t (Figure 2.5), were examined by finite element methods and compared with published empirical results[2] (Table 4.1). To obtain K_t from the finite element analysis, the maximum stress in the fillet adjacent to the shoulder with no external load is divided by the nominal stress. The difference between the empirical values and quadratic finite element values of K_t for the smaller bars ranges from 5.2 to 17.5 percent. These differences are attributed to the proximity of the unloaded shoulder to the external load. The streamline fillet (Figure 2.7) used on the unloaded shoulder of the 6.75 in. O.D. bar lowers the stress concentration factor by 22.6 percent. This type of fillet was derived by Grodinzinski[2] and is similar to the fillet suggested by Heywood for use on the loaded shoulder.

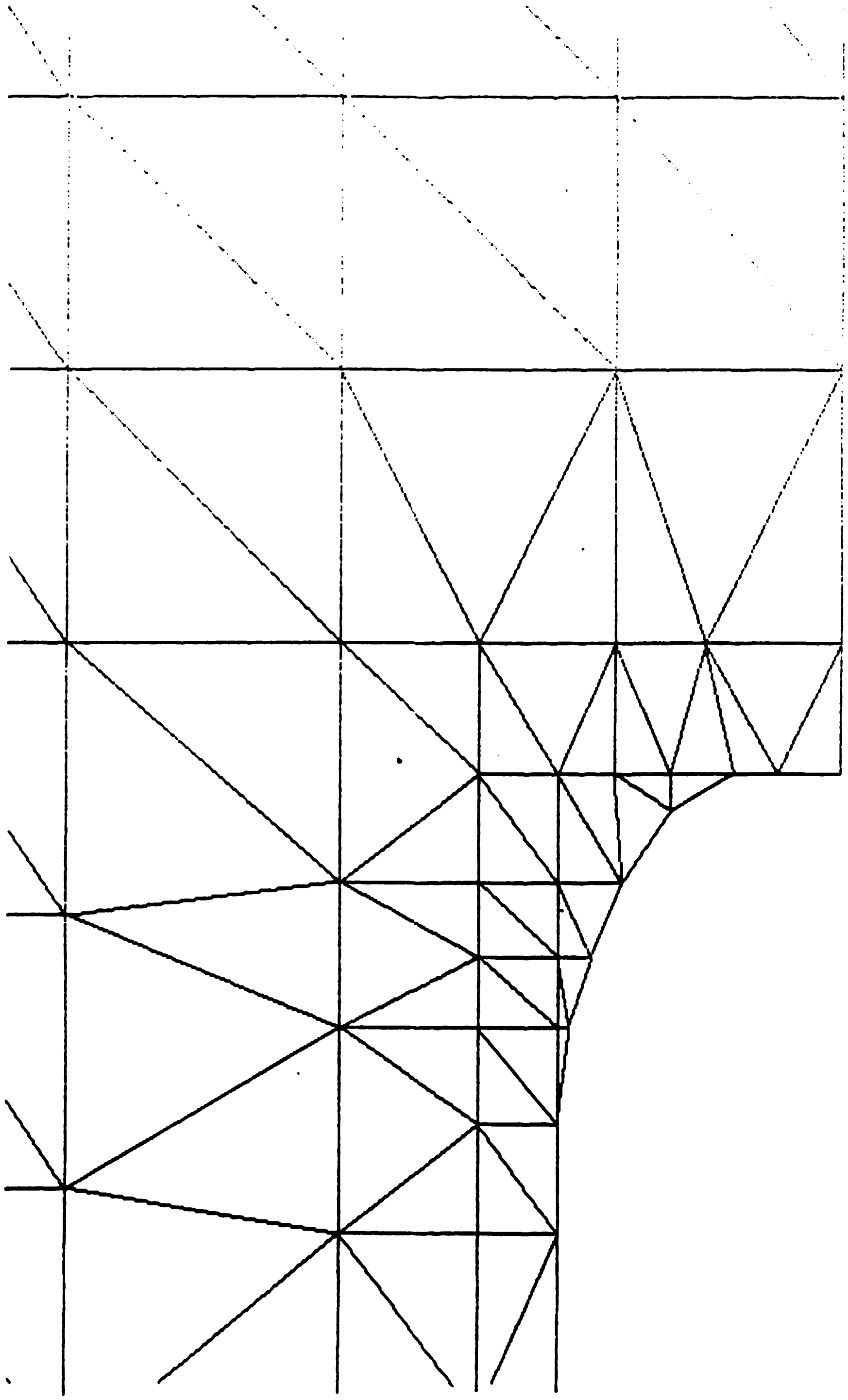

Figure 4.1a Detail of Streamline Fillet, 6.75 O.D.

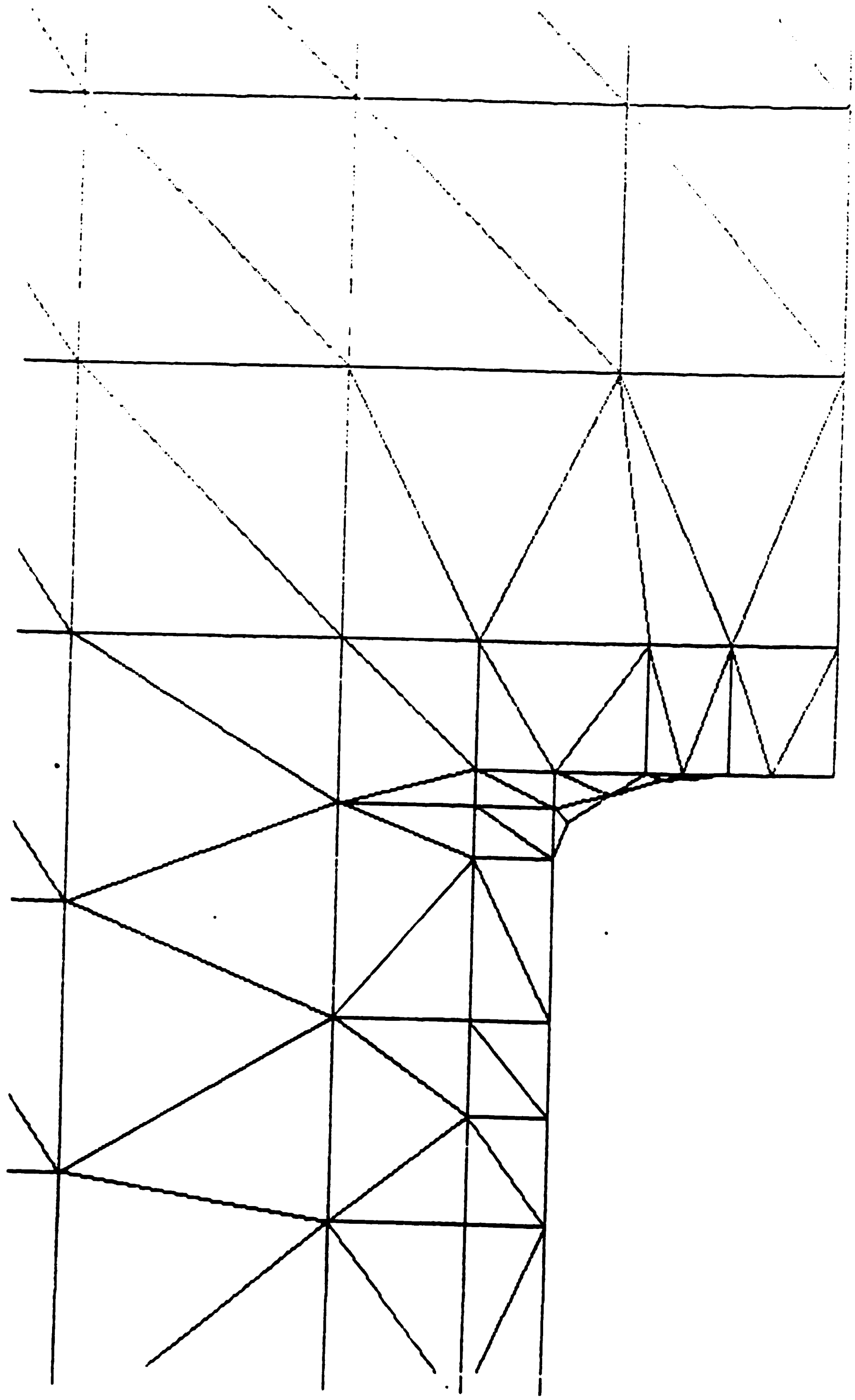

Figure 4.1b Detail of Reversed Streamline, 6.75 O.D.

4.2 THREADED BAR

The axial loaded stress concentration factors for threaded bars in tension, K_t (Figure 2.13), show poor correlation between the analytical values of Neuber[2] and the quadratic finite element values (Table 4.2). The differences range from 28.3 to 44.5 percent. K_t is obtained from the finite element analysis by putting the threaded bars under a tensile load (no thread load) and dividing the maximum stress by the nominal stress. Since the maximum difference between finite element values is reasonably small, it is assumed that the quadratic elements provide a good approximation of the stress concentration factors. This indicates that the analytical stress concentration factors of Neuber are too high.

The projection loaded stress concentration factors for threaded bars, K_o, show poor correlation between empirical results and quadratic finite element results. The differences range from 24.4 to 71.0 percent. These discrepancies have four possible sources. First, the values of K_t are used in the empirical formulations of K_o, and as noted in the previous paragraph the values of K_t appear to be in error. Second, Heywood included no correction factor in his empirical results for the threaded bars as he did for the grooved bars. Third, the grid used in the finite element analysis is not fine enough. Fourth, analytical methods are used to determine load distribution. The load distribution problem could be solved by modeling both the nut and the threaded bar in the finite element analysis. Both empirical and finite element methods yield results for K_o for the UNC bar that are higher than the accepted value of 2.7 (3.85 based on shank diameter) derived by Hetenyi by means of three dimensional photoelastic testing. Brown and Hickson obtained a value of 4.8 by performing similar experiments[2], while

Heywood obtained a value of 5.2 by empirical means[1]. This indicates that Hetenyi's results are low, and that the values in Table 4.2 form an upper and lower bound for K_o.

The Acme bar has higher values of K_o than the UNC bars because it has a greater load concentration at the first loaded thread. The application of Sopwith's results show that as the flank angle, β (Figure 2.10), of a thread becomes smaller, the load is distributed less uniformly.

4.3 TENSILE TESTING

Tensile tests conducted at Michigan State University on a Tinius-Olsen hydraulic tensile testing machine demonstrated that the stress concentrations calculated above are important only to the fatigue strength of the bars. Prior to testing, three material specimens (Figure 4.2) made out of the same steel (SAE 1018) as the tie bars modeled, were tested. The tensile force was measured by a load cell which monitored the hydraulic pressure in the tensile testing machine. The elongation of the specimen was measured by an extensometer. The electrical signals from the load cell and extensometer were fed into a strip chart recorder to construct a stress-strain diagram, from which the yield strength of the material was determined.

The model tie bars (Figure 4.3) were tested in the setup shown in Figure 4.4. The deflection Δ, was measured by an LVDT. Although Δ, was made up of the compression of the frame, bending of the collars, compression of the collars, stretch of the shank of the model, and stretch of the neck of the model, it was assumed that yielding would occur at the high stress areas indicated by the empirical and finite element procedures. The tensile force at the yield point could then

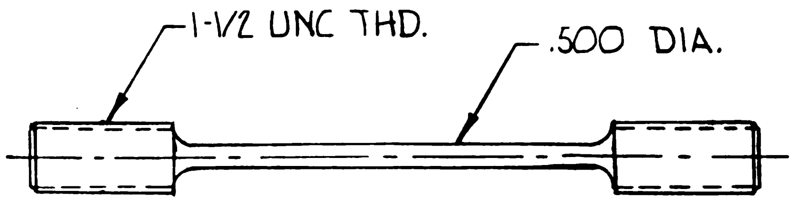

Figure 4.2 Material Specimen

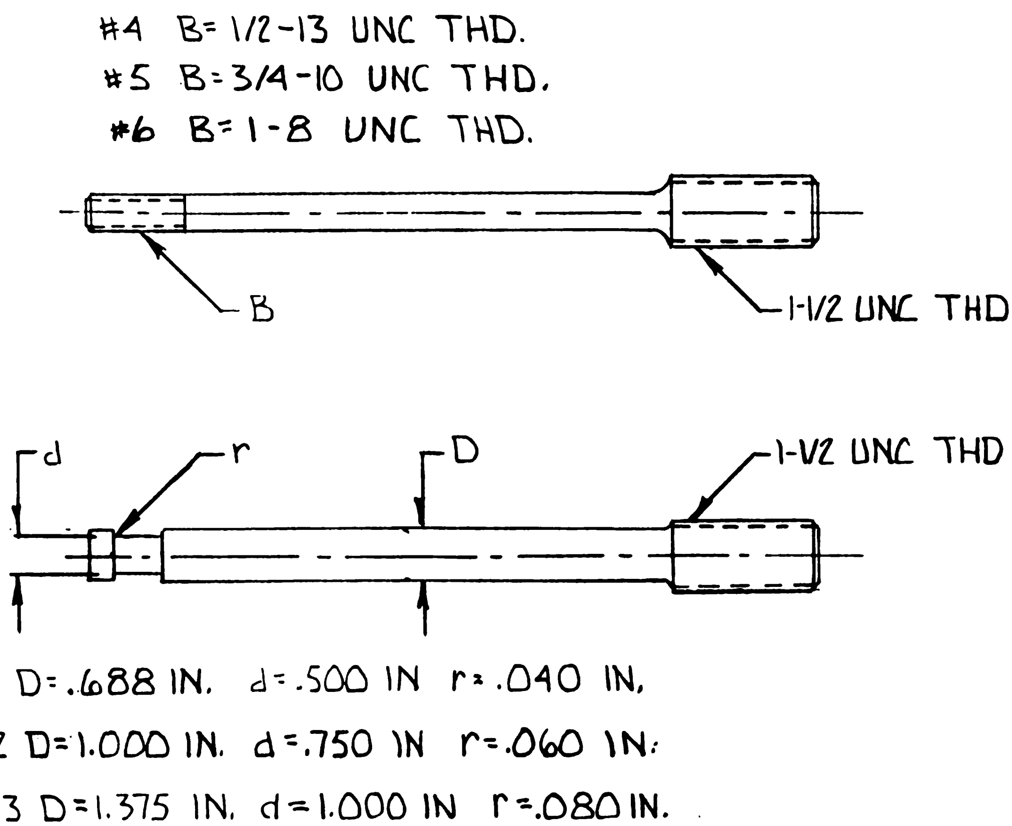

Figure 4.3 Model Tie Bars

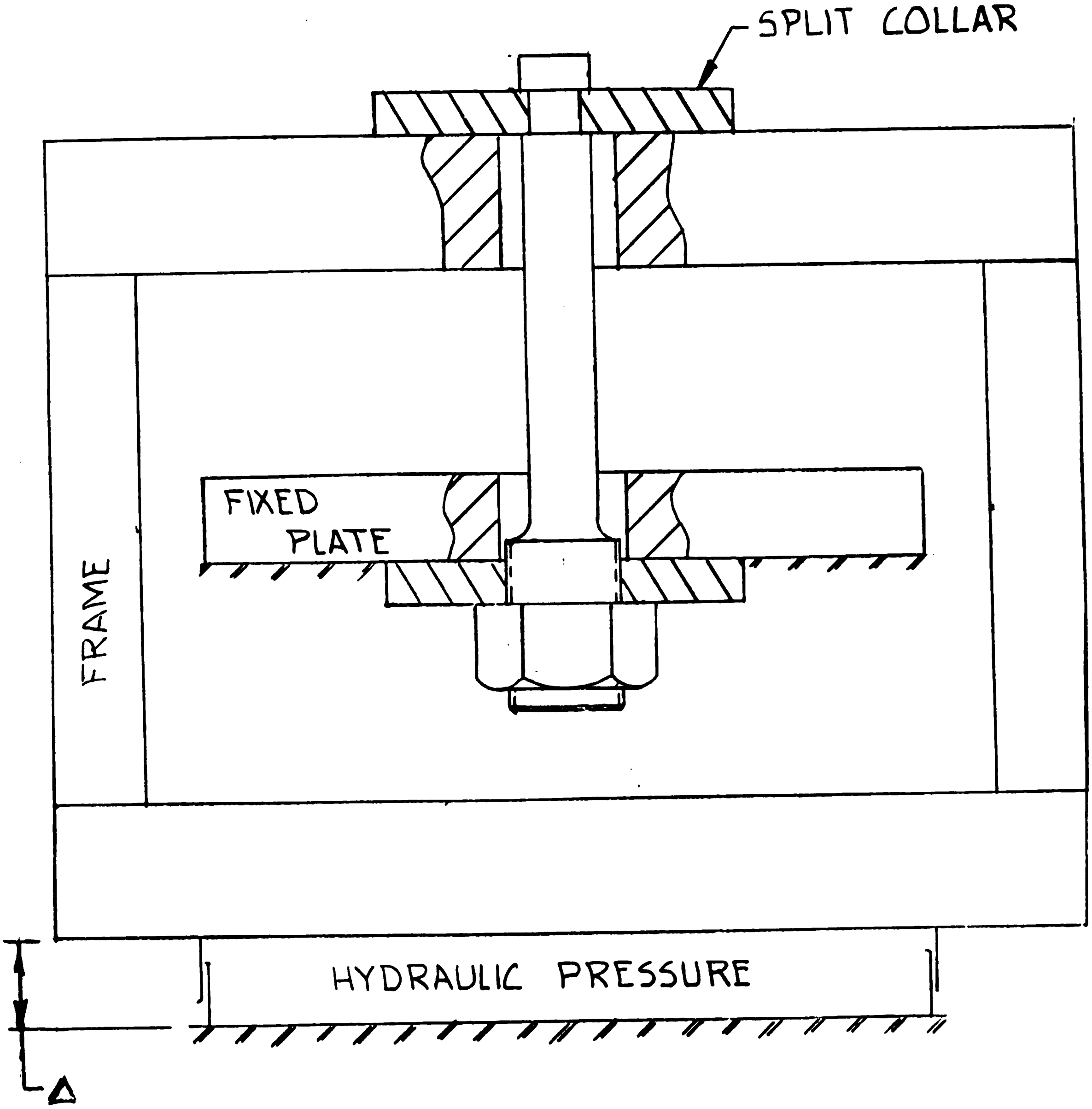

Figure 4.4 Testing Setup

be used with the already determined yield strength of the material to determine the stress concentration factor. This did not turn out to be. The finite element results show that the points of high stress are localized surface stresses. The ductile nature of the material used allowed the models to yield locally at the points of high stresses during the relatively static tensile test which eliminated the stress concentration factors. The location of yielding is shown in Figure 4.5.

These tensile tests confirm that the problem being studied is not of a static nature. If the tie bars had only steady loads on them, they would yield locally and all stress concentration factors would be eliminated. The tie bars however, are subjected to a cycling load. If the surface stresses exceed the material's fatigure strength, a surface crack will eventually occur which will propagate and cause failure.

4.4 FACTORS OF SAFETY

The maximum stress in the Acme threaded bar from the quadratic finite element analysis is 46,070 psi. This stress is the result of a 325,000 lb load, which corresponds to a 650 ton machine. Reducing this by 30 percent to account for a tapered nut would reduce the maximum stress to 35,440 psi. The stress concentration factor is 3.32 based on minor diameter. The Acme threaded bars are made of AISI 4140 steel with a hardness of R_c 19, a yield strength of 90,000 psi, and a tensile strength of 102,000 psi. The endurance level is estimated at 38,000 psi, using the machined surface curve of Figure 4.6[5]. The Soderberg equation, shown as Equation 4-3, is used to determine the factor of safety. It is based on the fact that the stress concentration should be applied to the alternating component of stress only[5].

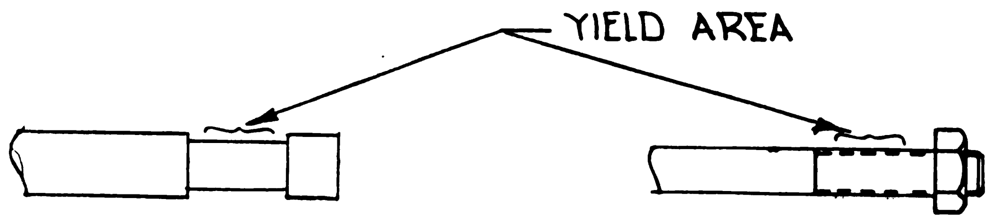

Figure 4.5 Location of Yielding

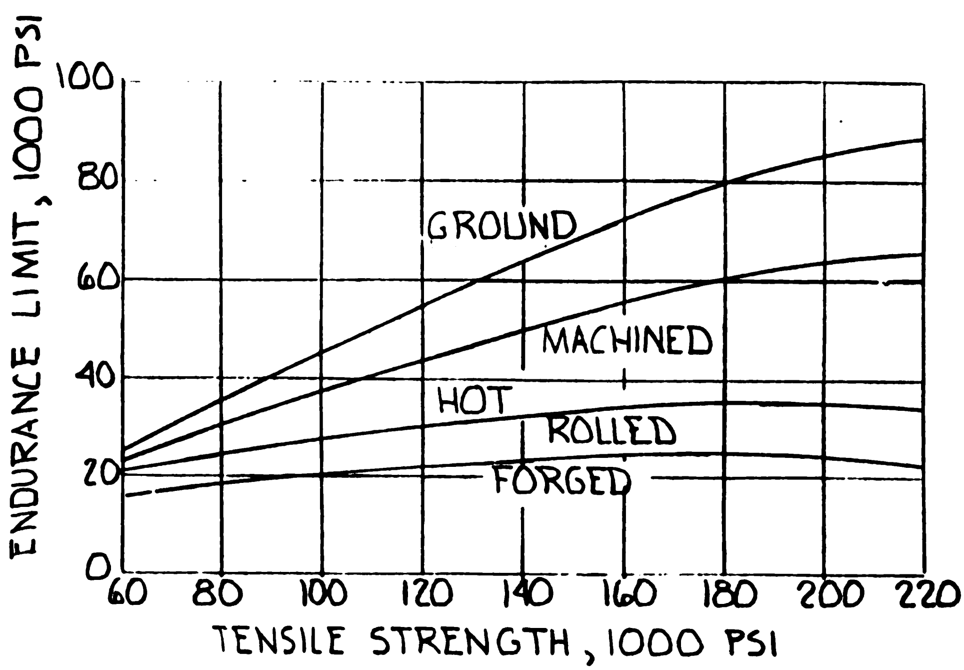

Figure 4.6 Endurance Limit

$$\sigma_{avg} + \frac{K_o \sigma_{yp}}{\sigma_e} \sigma_r = \frac{\sigma_{yp}}{F.S.} \qquad (4\text{-}3)$$

σ_{avg} = average nominal stress
σ_r = range of nominal stress from
σ_e = endurance limit
σ_{yp} = yield strength
F.S. = factor of safety

The factor of safety is calculated from Equation 4-3 to be 1.90. See Appendix D for calculations.

The maximum stress in the grooved bar with the streamline fillet from the quadratic finite element analysis is 47,340 psi. This stress is the result of a 300,000 lb load, which corresponds to a 600 ton machine. The stress concentration factor is 3.34 based on the minor diameter. The grooved bars are made of AISI 4340 with a hardness of R_c 34, a yield strength of 120,000 psi, and a tensile strength of 140,000 psi. The large size of the fillet allows it to be shot peened, which is beneficial in reducing fatigue cracks because it puts the surface in compression. Assuming that the shot peened surface is at least as good as the ground surface in resisting fatigue, the endurance level is estimated from Figure 4.6 to be 64,000 psi. The factor of safety is calculated from Equation 4-3 to be 2.34. See Appendix D for calculations.

Table 4.1 Empirical and Finite Element Stress Concentration Factors for Grooved Bars

K_o, Projection Loaded Stress Concentration Factor

Size	K_o Empirical	K_o Linear Finite Element	K_o Quadratic Finite Element
.688 O.D.	3.08	3.09	3.28
1.00 O.D.	3.12	3.25	3.30
1.38 O.D.	3.10	3.10	3.18
6.75 O.D. radius	3.05	3.10	3.48
6.75 O.D. streamline		3.07	3.34
6.75 O.D. reversed streamline		4.08	5.10

K_t, Axially Loaded Stress Concentration Factor

Size	K_t Chart	K_t Linear Finite Element	K_t Quadratic Finite Element
.688 O.D.	1.94	2.0	2.28
1.00 O.D.	1.92	1.91	2.16
1.38 O.D.	1.94	1.86	2.04
6.75 O.D. streamline	1.86	1.32	1.44

All K's Based On Minimum Diameter

All Dimensions In Inches

Table 4.2 Empirical and Finite Element Stress Concentration Factors for Threaded Bars

K_o, Projection Loaded Stress Concentration Factor

Size	K_o Empirical	K_o Linear Finite Element	K_o Quadratic Finite Element
1/2-13	4.95	3.41	3.74
3/4-10	5.34	3.64	3.79
1-8	5.38	3.49	3.73
Acme	14.9	4.63	4.32

K_t, Axially Loaded Stress Concentration Factor

Size	K_t Chart	K_t Linear Finite Element	K_t Quadratic Finite Element
1/2-13	3.07	2.60	2.20
3/4-10	3.25	2.60	2.20
1-8	3.26	2.34	2.07
Acme	2.99	1.50	1.66

All K's Based On Minimum Diameter

All Dimensions In Inches

CHAPTER FIVE

CONCLUSIONS

The stresses in threaded and grooved tie bars were analyzed using the analytical and empirical methods of Sopwith, Neuber, and Heywood, and by finite element methods. The stresses were used to calculate stress concentration factors which are tabulated in Tables 4.1 and 4.2. The stress concentration factors were used in Soderberg's Equation to calculate factors of safety (Section 4.4).

Two finite element programs were used to analyze stresses in the two types of bars. One program used linear elements, the other quadratic elements. Linear elements have constant displacement gradients which result in constant stresses within each element. The quadratic elements allow the stresses to vary linearly within the element. The same grid was used for the two programs so the trends of the results could be observed when the more accurate quadratic elements were used.

The finite element analysis and tensile testing of model tie bars showed that the maximum stresses that were calculated are local surface stresses and therefore only important for fatigue calculations.

The grooved bar projection loaded stress concentration factors, K_o, have lower empirical values than quadratic finite element values

(Table 4.1). The correction factor Heywood used for bar geometries of this type appears to be incorrect because the stress concentration factors increase when the more accurate quadratic elements are used. Two other fillet designs were tried in order to attempt to lower the stresses obtained with the radius fillet. The first was a streamline fillet (Figure 4.1a) suggested by Heywood. The finite element analysis showed this type of fillet to be ineffective in lowering stresses because of the small radius near the load. A reversed streamline (Figure 4.1b) was tried in order to place a large radius near the load, but the maximum stress increased because of the small radius at the bottom of the fillet. Based on the finite element results a radius fillet appears to be the best design for this bar geometry and loading.

The grooved bar axial loaded stress concentration factors, K_t (Figure 2.5), have higher finite element values than previously published empirical values[2] (Table 4.1), because of the proximity of the unloaded shoulder to the external load. The finite element analysis confirmed that the streamline fillet is effective in reducing stresses in axially loaded shoulder shafts.

Application of Sopwith's results showed that the UNC thread is superior to the Acme thread in the distribution of load because of the greater flank angle β, of the UNC thread (Figure 2.10).

The threaded bar axial loaded stress concentration factors, K_t, have lower finite element values than the analytical values of Neuber[1] (Table 4.2). The relatively small variation observed when comparing linear and quadratic finite element values indicated that the use of a finer grid or higher order elements would not significantly effect the

the accuracy of the results. This indicated that the analytical stress concentration factors of Neuber are too high.

The UNC threaded bar projection loaded stress concentration factors, K_o, have higher empirical and finite element values than the generally accepted value derived by Hetenyi. This supports Heywood, Brown, and Hickson who also disputed Hetenyi's results. Because of this, the results in Table 4.2 appear to form an upper and lower bound for K_o.

The results presented here show that the accepted stress concentration factor for projection loaded UNC threaded bars is too low. Since this stress concentration factor is of importance to many industries, it is imperative that further finite element research be done, modeling the nut and bar toether to solve the problem of load distribution, and using finer grids or higher order elements to insure accuracy.

APPENDICES

APPENDIX A

DERIVATION OF BENDING STRESS TERM

$$\sigma_b' = \frac{My}{I}$$

M = Moment = Pa
y = Distance From Neutral Axis = e
I = Moment of Inertia

$$\sigma_b' = \frac{P(a)e}{1/12(t)(2e)^3} = \frac{Pae}{2/3(t)e^3} = \frac{1.5a}{e^3}\left(\frac{P}{t}\right)$$

APPENDIX B

GROOVED TIE BAR CALCULATIONS

See Figure 2.4 for Definition of Dimensions

$a = b = (D\ d)/4$
$e = 1/2(m+r(1-\cos 30))$
P = Load
All Dimensions in Inches

BAR #1

$m = .385$

$d = .500$

$D = .688$

$r = .040$

$a = b = .047$

$e = .195$

$\beta = \gamma = 0$

$\sigma_b = 13.7P$ See Equation 2-4

$K_t = 1.94$ See Figure 2.5

$\sigma_t = 9.88P$ See Equation 2-5

$c = 1.86$ See Equation 2-7

$\sigma_c = 15.7P$ See Equation 2-6

$K_o = 3.08$ Based on d

BAR #2

$m = .562$

$d = .750$

$D = 1.00$

$r = .060$

$a = b = .0625$

$e = .285$

$\beta = \gamma = 0$

$\sigma_b = 6.26P$ See Equation 2-4

$K_t = 1.92$ See Figure 2.5

$\sigma_t = 4.35P$ See Equation 2-5

$c = 1.86$ See Equation 2-7

$\sigma_c = 7.08P$ See Equation 2-6

$K_o = 3.12$ Based on d

BAR #3

$m = .750$

$d = 1.00$

$D = 1.38$

$r = .080$

$a = b = .0938$

$e = .380$

$\beta = \gamma = 0$

$\sigma_b = 3.45P$ See Equation 2-4

$K_t = 1.94$ See Figure 2.5

$\sigma_t = 2.47P$ See Equation 2-5

$c = 1.86$ See Equation 2-7

$\sigma_c = 3.95P$ See Equation 2-6

$K_o = 3.10$ Based on d

BAR #4

$m = 3.61$

$d = 5.20$

$D = 6.75$

$r = .482$

$a = b = .388$

$e = 1.84$

$\beta = \gamma = 0$

$\sigma_b = .128P$ See Equation 2-4

$K_t = 1.86$ See Figure 2.5

$\sigma_t = .0878P$ See Equation 2-5

$c = 1.86$ See Equation 2-7

$\sigma_c = .144P$ See Equation 2-6

$K_o = 3.05$ Based on d

APPENDIX C

THREADED TIE BAR CALCULATIONS

See Figures 2.2 and 2.10 for Definitions of Dimensions

$\mu = .2$ Coefficient of Friction
$\sigma = .3$ Poisson's Ratio
All Dimensions in Inches

$$T = \frac{2}{1 + \cos 2\beta + \sin 2\beta} \tag{C-1}$$

$$B_1 = \frac{2\left(\frac{2\sin 2\beta}{2\beta - \sin 2\beta} + T\right)}{2\beta + \sin 2\beta} \tag{C-2}$$

$$B_2 = \frac{2}{2\beta - \sin 2\beta} + \frac{1 - 2\sigma}{(1-\sigma)\sin 2\beta} - 2T\frac{1 - \cos 2\beta}{\sin 2\beta - 2\beta\cos 2\beta} \tag{C-3}$$

$$B_3 = \frac{2T}{\sin 2\beta - 2\beta\cos 2\beta} \tag{C-4}$$

$$z - \frac{x+h}{x} \tag{C-5}$$

$$q - (1 - \sigma^2)[B_1 \ln(z) - \frac{z-1}{z}(B_2 + B_3 \frac{z-1}{z})] \tag{C-6}$$

$$U = \frac{(\tan\beta) - \mu}{(\cot\beta) - \mu} + 2q\frac{w(D_3^2 - D_m^2)}{(D_m)(D_3)^2} \tag{C-7}$$

$$V = 1/2\sigma\tan\beta \qquad \text{(C-8)}$$

$$\theta_2 = \frac{2L\sqrt{U+V^2}}{UD_m} \qquad \text{(C-9)}$$

$$\lambda = \frac{V}{\sqrt{U+V^2}} \qquad \text{(C-10)}$$

$$H = \theta_2(\coth(\theta_2) - \lambda) \qquad \text{(C-11)}$$

BAR #5 (1/2-13)

$w = .0769$	$D_m = .453$	$r = .0115$	$\gamma = 11.3°$
$x = .483$	$D = .500$	$a = .500$	$d_m = .406$
$h = .0472$	$D_3 = .750$	$b = .0243$	$\beta = .524$ rad.
$L = .484$	$e = .0333$		

$T = 1.20$
$B_1 = 11.2$
$B_2 = 8.21$
$B_3 = 6.98$
$z = 1.71$
$q = 1.29$ — See Equations C-1 To C-11
$U = .474$
$V = .0866$
$\lambda = .125$
$\theta_2 = 3.13$
$H = 2.75$

$(R/t)_{avg} = .125R$	See Equation 2-9
$(R/t)_{max} = .343R$	See Equation 2-10
$R = 1.056P$	See Equation 2-8
$\sigma_b = 21.8P$	See Equation 2-11
$\delta = .55$	See Figure 2.12
$K_t = 3.20$	See Figure 2.13
$K_c = 3.07$	See Equation 2-13
$\sigma_t = 23.8P$	See Equation 2-14
$c = .465$	See Equation 2-16

$\sigma_c = 38.2P$ See Equation 2-15
$K_o = 4.95$ Based on d_m

BAR #6 (3/4-10)

$w = .100$	$D_m = .689$	$r = .0141$	$\gamma = 11.3$
$x = .0866$	$D = .750$	$a = .0177$	$d_m = .627$
$h = .0613$	$D_3 = 1.25$	$b = .0333$	$\beta = .524$ rad.
$L = .734$	$e = .0427$		

$R = 1.20$
$B_1 = 11.2$
$B_2 = 8.21$
$B_3 = 6.98$
$r = 1.71$
$q = 1.29$ — See Equations C-1 To C-11
$U = .456$
$V = .0866$
$\lambda = .127$
$\theta_2 = 3.18$
$H = 2.79$

$(R/t)_{avg} = .0691R$ See Equation 2-9
$(R/t)_{max} = .193R$ See Equation 2-10
$R = 1.056P$ See Equation 2-8
$\sigma_b = 9.96P$ See Equation 2-11
$\delta = .55$ See Figure 2.12
$K_t = 3.40$ See Figure 2.13
$K_c = 3.25$ See Equation 2-13
$\sigma_t = 10.5P$ See Equation 2-14
$c = .465$ See Equation 2-16
$\sigma_c = 17.2P$ See Equation 2-15
$K_o = 5.34$ Based on d_m

BAR #7 (1-8)

$w = .125$	$D_m = .923$	$r = .0177$	$\gamma = 11.3^\circ$
$x = .108$	$D = 1.00$	$a = .0220$	$d_m = .847$
$h = .0767$	$D_3 = 1.62$	$b = .0407$	$\beta = .524$ rad.
$L = .981$	$e = .0540$		

$T = 1.20$
$B_1 = 11.2$
$B_2 = 8.21$
$B_3 = 6.98$
$z = 1.71$
$q = 1.29$ — See Equations C-1 To C-11
$U = .432$
$V = .0866$
$\lambda = .131$
$\theta_2 = 3.27$
$H = 2.85$

$(R/t)_{avg} = .0477R$	See Equation 2-9
$(R/t)_{max} = .136R$	See Equation 2-10
$R = 1.056P$	See Equation 2-8
$\sigma_b = 5.58P$	See Equation 2-11
$\delta = .55$	See Figure 2.12
$K_t = 3.40$	See Figure 2.13
$K_c = 3.26$	See Equation 2-13
$\sigma_t = 5.78P$	See Equation 2-14
$c = .465$	See Equation 2-16
$\sigma_c = 9.55P$	See Equation 2-15
$K_o = 5.38$	Based of d_m

BAR #8 (Acme Thread)

$w = .250$	$D_m = 6.36$	$r = .0200$	$\gamma = 11.3°$
$x = .483$	$D = 6.50$	$a = .058$	$r' = .0562$
$h = .135$	$D_3 = 10.2$	$b \doteq .064$	$d_m = 6.23$
$\beta = .253$ rad.	$L = 6.75$	$e = .08$	

$T = 1.011$
$B_1 = 94.4$
$B_2 = 89.6$
$B_3 = 47.8$
$z = 1.28$
$q = 1.29$ — See Equations C-1 To C-11
$U = .0764$
$V = .0388$
$\lambda = .134$
$\theta_2 = 7.75$
$H = 6.67$

$(R/t)_{avg} = .00187R$	See Equation 2-9
$(R/t)_{max} = .0126R$	See Equation 2-10
$R = 1.002P$	See Equation 2-8
$\sigma_b = .477P$	See Equation 2-11
$\delta = .55$	See Figure 2.12
$K_t = 3.00$	See Figure 2.13 Use r', See Figure 2.10
$K_c = 2.99$	See Equation 2-13
$\sigma_t = .0981P$	See Equation 2-14
$c = 1.07$	See Equation 2-16
$\sigma_c = .489P$	See Equation 2-15
$K_o = 14.9$	Based on d_m

APPENDIX D

CALCULATION OF FACTOR OF SAFETY

ACME THREADED BAR

Minor diameter = 6.23 in

$P_{avg} = (P_{max} + P_{min})/2 = (325{,}000 + 0)/2 = 162{,}500$ lb

$P_r = P_{max} - P_{avg} = 325{,}000 - 162{,}500 = 162{,}500$ lb

$$\sigma_{avg} = \frac{P_{avg}}{\pi(d_m/2)^2} = \frac{162{,}500}{\pi(3.115)^2} = 5330 \text{ psi} \quad \text{nominal stress}$$

$$\sigma_r = \frac{P_r}{\pi(d_m/2)^2} = \frac{162{,}500}{\pi(3.115)^2} = 5330 \text{ psi} \quad \text{nominal stress}$$

$\sigma_e = 38{,}000$ psi

$\sigma_{yp} = 90{,}000$ psi

$K_o = 3.32$ (obtained by reducing 4.32 by 30%)

Using Equation 4-3 F.S. = 1.90

GROOVED BAR

Minor diameter = 5.195 in

$P_{avg} = (300{,}000 + 0)/2 = 150{,}000$ lb

$P_r = 300{,}000 - 150{,}000$ lb

$$\sigma_{avg} = \frac{150,000}{\pi(2.598)^2} = 7070 \text{ psi} \quad \text{nominal stress}$$

$$\sigma_r = \frac{150,000}{\pi(2.598)^2} = 7070 \text{ psi} \quad \text{nominal stress}$$

$\sigma_e = 64,000$ psi

$\sigma_{yp} = 120,000$ psi

$K_o = 3.34$

Using Equation 5-3 F.S. = 2.34

APPENDIX E

COMPUTER MATRICES AND LINEAR SHAPE FUNCTIONS

$$\{\sigma\}^T = [\sigma_{rr}\ \sigma_{zz}\ \sigma_{\theta\theta}\ \tau_{rz}]$$

$$[D] = \frac{E(1-\sigma)}{(1+\sigma)(1-2\sigma)} \begin{bmatrix} 1 & \frac{\sigma}{1-\sigma} & \frac{\sigma}{1-\sigma} & 0 \\ \frac{\sigma}{1-\sigma} & 1 & \frac{\sigma}{1-\sigma} & 0 \\ \frac{\sigma}{1-\sigma} & \frac{\sigma}{1-\sigma} & 1 & 0 \\ 0 & 0 & 0 & \frac{1-2\sigma}{2(1-\sigma)} \end{bmatrix}$$

where E = Elastic Modulus
σ = Poisson's Ratio

$$\{\varepsilon_o\} = \alpha\Delta T \begin{bmatrix} 1 \\ 1 \\ 1 \\ 0 \end{bmatrix}$$

where α = Coefficient of Thermal Expansion
ΔT = Change in Temperature

$$[B] = \frac{1}{2A} \begin{bmatrix} b_i & 0 & b_j & 0 & b_k & 0 \\ 0 & c_i & 0 & c_j & 0 & c_k \\ \frac{2AN_i}{r} & 0 & \frac{2AN_j}{r} & 0 & \frac{2AN_k}{r} & 0 \\ c_i & b_i & c_j & b_j & c_k & b_k \end{bmatrix}$$

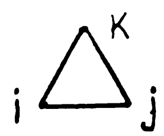

TYPICAL ELEMENT

where N's = Shape Functions

$$b_p = \frac{\partial N_p}{\partial r} \quad p = i,j,k$$

$$c_p = \frac{\partial N_p}{\partial z} \quad p = i,j,k$$

A = Element Area
r = Centroidal Radius

$$N_p = \frac{1}{2A}[a_p + b_p r + c_p z] \quad p = i,j,k$$

$$a_i = r_j z_k - r_k z_j$$

$$b_i = z_j - z_k$$

$$c_i = r_k - r_j$$

$$a_j = r_k z_i - z_k r_i$$

$$b_j = z_k - z_i$$

$$c_j = r_i - r_k$$

$$a_k = r_i z_j - r_j z_i$$

$$b_k = z_i - z_j$$

$$c_k = r_j - r_i$$

BIBLIOGRAPHY

BIBLIOGRAPHY

[1] R.B. Heywood, Designing By Photoelasticity. London: Chapman & Hall, 1952.

[2] R.E. Peterson, Stress Concentration Design Factors. New York: Wiley, 1974.

[3] L.J. Segerlind, Applied Finite Element Analysis. New York: Wiley, 1976.

[4] D.G. Sopwith, "The Distribution of Load in Screw Threads," IME Proceedings, vol. 159, pp. 373-383, 396-397, 1948.

[5] M.F. Spotts, Design of Machine Elements. Englewood Cliffs, New Jersey: Prentice Hall, 1978.